SSC-217

COMPRESSIVE STRENGTH OF SHIP HULL GIRDERS PART I UNSTIFFENED PLATES

This document has been approved for public release and sale; its distribution is unlimited.

SHIP STRUCTURE COMMITTEE

1970

SHIP STRUCTURE COMMITTEE

AN INTERAGENCY ADVISORY
COMMITTEE DEDICATED TO IMPROVING
THE STRUCTURE OF SHIPS

MEMBER AGENCIES:

UNITED STATES COAST GUARD
NAVAL SHIP SYSTEMS COMMAND
MILITARY SEALIFT COMMAND
MARITIME ADMINISTRATION
AMERICAN BUREAU OF SHIPPING

ADDRESS CORRESPONDENCE TO:

SECRETARY
SHIP STRUCTURE COMMITTEE
U.S. COAST GUARD HEADQUARTERS
WASHINGTON, D.C. 20591

1970

Dear Sir:

The Ship Structure Committee has a continuing interest in the ultimate strength of ship hull structural components. In connection with this, research has been sponsored investigating the strength of small structural models under various combinations of longitudinal, transverse and normal loads.

The results of the first phase of this project are reported herein.

Sincerely,

W. F. REA, III
Rear Admiral, U.S. Coast Guard
Chairman, Ship Structure Committee

SSC-217
Technical Report
on
Project SR-193, "Small Hull Girder Model"

COMPRESSIVE STRENGTH OF SHIP HULL GIRDERS
PART I
UNSTIFFENED PLATES

by
H. Becker, R. Goldman, J. Pazerycki
Mithras

under
Department of the Navy
Naval Ship Engineering Center
Contract No. N00024-69-C-5413

This document has been approved for public release and sale; its distribution is unlimited.

U.S. Coast Guard Headquarters
Washington, D.C.
1970

ABSTRACT

This is Part I of a two-part report on a year of investigation into the compressive strength of ship hull girders. This Part covers unstiffened plates while Part II will cover stiffened plates.

Three problem areas of Hull girder strength are biaxial strength (to account for the transverse membrane loadings induced by the sea), the influence of normal pressure loadings on strength, and the influence on strength of residual stresses induced by welding. Data on solutions to these problems were obtained during this project.

1. Tests reveal a large reduction in the longitudinal strength of a plate when transverse membrane loading is applied for plates with b/t = 30 and 50. This result agrees with the prediction in the Feasibility Study that preceded this investigation (Ref. 1).

2. Hypotheses have been evolved for determining the biaxial strength of plates. They are in general agreement with the experimental data.

3. Experiments were conducted on wide column strength, the results of which agree with theoretical predictions.

4. It was demonstrated that normal pressure up to 11 psi exerts a negligible influence on the longitudinal strength of plates, which agrees with indications presented in Ref. 1. The same is true for transverse and biaxial strengths for b/t = 30 and 50. However, pressure was observed to induce a moderate reduction in biaxial strength for b/t = 70 and a 40 percent reduction for b/t = 90.

5. A theory was developed for predicting the influence of weld-induced residual stresses on plate strength. It was found to correlate well with current experimental results and is in agreement with similar tests on large scale plates (Ref. 2). The theory showed that the strength-affecting proportion of plate residual stress should decrease with b/t and essentially vanish in steels at b/t = 30, although the actual residual increases rapidly with decreasing b/t.

6. A foundation was established for predicting the weld-induced loss in plate strength from knowledge of the welding parameters that control the residual stress field in the plate. Furthermore, stresses were measured at weld centerlines and were found to exceed the material yield.

7. It was demonstrated that the older design chart for uniaxial strength of plates may be optimistic compared to the mass of more recent data.

CONTENTS

NOMENCLATURE

Symbols

a	length of plate, in.
b	width of plate, in. (outside dimensions of tube)
b_e	effective width of equivalent flange, in.
D	bending stiffness of plate, $Et^3/[12(1-\nu^2)]$, in-lb.
E	Young's modulus, msi (1 msi = 10^6 psi)
E_s, E_t	secant and tangent moduli, msi
F	$(t/b)(E/\sigma_{cy})^{1/2}$
g	multiplier converting σ_{cy} to σ_e
h	number of effective transverse flanges in a plate at biaxial failure
k_x	longitudinal buckling coefficient
k_y	transverse buckling coefficient
ℓ	multiplier for converting plate thickness (t) to effective width of weld tension stress region on one side of weld centerline, in.
m	number of longitudinal half waves in buckled plate
N_x	plate longitudinal loading, $t\sigma_x$, lb/in.
N_y	plate transverse loading, $t\sigma_y = 0.707\ P_y/a$, lb/in.
P_x	force applied longitudinally to tube, lb.
P_y	force applied diagonally transverse to tube, lb.
P_2	equivalent force developable by pair of effective flanges at yield, $2b_e t\sigma_{cy}$, lb.
p	pressure acting normal to plate, psi

s	parameter in theoretical relation for uniaxial longitudinal strength
t	thickness of plate, in.
V	shear force in residual stress field, lb.
w	deflection normal to prebuckling plane of plate, in.
w_o	central deflection normal to prebuckling plane of plate, in.
x	longitudinal coordinate of plate, in.
y	transverse coordinate of plate, in.
α	effectiveness factor for residual stresses
ϵ	strain
η	plasticity reduction factor for inelastic buckling
ν	Poisson's ratio
σ	stress, ksi

Subscripts

e	along edge of plate (also elastic when referring to ν)
r	residual, or related to residual stress
u	ultimate
x, y, z	coordinate directions
cr	critical, or buckling
cy	compressive yield (in this report a reference to yield is always identified as compressive yield)

Combined subscripts may be formed from the above. For example:

x cr	x-direction (or longitudinal) critical or buckling
yu	y-direction (or transverse) ultimate

SHIP STRUCTURE COMMITTEE

The SHIP STRUCTURE COMMITTEE is constituted to prosecute a research program to improve the hull structures of ships by an extension of knowledge pertaining to design, materials and methods of fabrication.

RADM W. F. Rea, III, USCG, Chairman
Chief, Office of Merchant Marine Safety
U. S. Coast Guard Headquarters

Capt. J. E. Rasmussen, USN
Naval Ship Engineering Center
Prince Georges' Center Building

Capt. T. J. Banvard, USN
Maintenance and Repair Officer
Military Sealift Command

Mr. E. S. Dillon
Chief
Office of Ship Construction
Maritime Administration

Mr. C. J. L. Schoefer, Vice President
American Bureau of Shipping

SHIP STRUCTURE SUBCOMMITTEE

The SHIP STRUCTURE SUBCOMMITTEE acts for the Ship Structure Committee on technical matters by providing technical coordination for the determination of goals and objectives of the program, and by evaluating and interpreting the results in terms of ship structural design, construction and operation.

NAVAL SHIP ENGINEERING CENTER

Mr. P. M. Palermo - Chairman
Mr. J. B. O'Brien - Contract Administrator
Mr. G. Sorkin - Member
Mr. H. S. Sayre - Alternate
Mr. I. Fioriti - Alternate

MARITIME ADMINISTRATION

Mr. F. Dashnaw - Member
Mr. A. Maillar - Member
Mr. R. Falls - Alternate
Mr. Raymond F. Coombs - Alternate

AMERICAN BUREAU OF SHIPPING

Mr. S. G. Stiansen - Member
Mr. F. J. Crum - Member

OFFICE OF NAVAL RESEARCH

Mr. J. M. Crowley - Member
Dr. W. G. Rauch - Alternate

NAVAL SHIP RESEARCH & DEVELOPMENT CENTER

Mr. A. B. Stavovy - Alternate

MILITARY SEALIFT COMMAND

Mr. R. R. Askren - Member
Lt. J. G. T. E. Koster, USN, - Member

U. S. COAST GUARD

LCDR C. S. Loosmore, USCG - Secretary
CDR C. R. Thompson, USCG - Member
CDR J. W. Kime, USCG - Alternate
CDR J. L. Coburn - Alternate

NATIONAL ACADEMY OF SCIENCES

Mr. R. W. Rumke, Liaison
Prof. R. A. Yagle, Liaison

SOCIETY OF NAVAL ARCHITECTS & MARINE ENGINEERS

Mr. T. M. Buermann, Liaison

AMERICAN IRON AND STEEL INSTITUTE

Mr. J. R. Lecron, Liaison

BRITISH NAVY STAFF

Dr. V. Flint, Liaison
CDR P. H. H. Ablett, RCNC, Liaison

WELDING RESEARCH COUNCIL

Mr. K. H. Koopman, Liaison
Mr. C. Larson, Liaison

INTRODUCTION

Aims of the Project

The purpose of the square tube tests was to obtain a large quantity of experimental data on the ultimate strength of rectangular plates under various combinations of longitudinal membrane loading (N_x), transverse membrane loading (N_y), and normal pressure (p). Furthermore, it is the intent of this project to support the experimental data with theoretical explanations.

The use of square tubes is one of a number of ways in which plates can be tested under uniaxial compression. The continuity across each edge of the tube simulates the behavior of plates in a ship. The ultimate load behavior of a longitudinally stiffened bottom would be reproduced in the tubes and therefore little doubt should exist concerning the direct applicability of the results to naval architecture. In addition, it was pointed out in Ref. 1 that there is no scale factor in structural stability experiments. This was demonstrated in the residual stress studies of this investigation.

On the basis of these considerations, therefore, it is felt that the current studies have satisfied the aims of the project.

State of the Art

A detailed review was presented (Ref. 1) of the state of the art before this investigation began. A summary appears in Table 1. The advancements in the status, resulting from this investigation, are indicated by X at several positions in the table. A resume of the specific accomplishments of the current studies appears in the summary of this report. The results of Dwight and Ractliffe (Ref. 2) provide an important recent input to the available information. Furthermore, their results were obtained on large plates and thereby provide a direct test of scale effects on stability for many of the studies performed in the current effort.

Experimental data on biaxial compression strength presumably are reported here for the first time. No test results on this problem have been seen before. In addition, the influence of normal pressure on biaxial compression strength was examined experimentally.

Terminology

Several terms are used in this report to identify instability. "Buckling" and "critical" are synonymous. They refer to the change from the flat to the bent state in accordance with the classical notions of instability. For edge-supported flat plates this change is seldom sharp. In actuality, it marks a load range in which a visible wave pattern begins to form and starts to deepen into the geometric configuration commonly termed "a buckle".

Table I.
Status of Theory and Experiment on Pertinent[1] Features of Plate Buckling and Strength Data

	Feature	Quantity	Theory	Experiment
Zero Pressure	Uniaxial Comp.	σ_{cr}	Extensive	Extensive
		σ_u	Yes X	Yes X
	Biaxial Comp.	σ_{cr}	Yes	No
		σ_u	No X	No X
Finite Pressure	Uniaxial Comp.	σ_{cr}	Yes	Yes
		σ_u	No	No X
	Biaxial Comp.	σ_{cr}	No	No
		σ_u	No	No X
Effects of Residual Stress			Yes X	Yes X

[1] Yes - Data exist from previous studies. No - No published previous data. X-Current contribution.

"Maximum", "ultimate" and "failure" are synonyms which pertain to the upper extreme of the load carrying capability of a structure. They may refer to a test value, or to a property of the structure. In this report the usage of these three terms is confined to test values.

The preceding terms may be either adjectives or nouns, depending upon the idiomatic usage. "Strength", however, is a noun only. It is a property of the structure, and is not a test value. It is the magnitude of the upper limit of load carrying capacity of a structure implying the existence of an associated numerical value and is only indirectly a state descriptor.

STABILITY THEORIES AND HYPOTHESES

Buckling

The differential equation for buckling of a flat plate is (Ref. 3)

$$\partial^4 w/\partial x^4 + 2\partial^4 w/\partial x^2 \partial y^2 + \partial^4 w/\partial y^4 + (N_x/D)\,\partial^2 w/\partial x^2 + (N_y/D)\partial^2 w/\partial y^2 = 0 \qquad (1)$$

for which the general biaxial compressive buckling solution may be chosen in the form

$$w = w_o \sin(m\pi x/a)\sin(n\pi y/b) \qquad (2)$$

For narrow column buckling there is only one half wave in the y direction and none in the x direction. Furthermore, $N_{xy} = 0$. These situations also apply reasonably well to a wide column. Consequently the x-dependent component of the deflection is discarded and a simplified solution to Eq. (1) for wide column buckling is

$$w = w_o \sin(\pi y/b) \tag{3}$$

It follows that the longitudinal component of any compression residual stress (which exists across almost the entire width of the plate) would not influence wide column buckling. It also implies that residuals would have a relatively small effect upon the N_y buckling of a simply supported plate with $a/b = 3$.

The preceding is a reasonably good solution to the wide column buckling problem. However, it is more precisely limited to a lineal element since it does not account properly for the anticlastic curvature at the free edges. It is necessary to utilize the precise deflection function provided by Timoshenko for plates with various boundary conditions (Ref. 3). The wide column solution agrees with Eq. (3) but no solution is provided for the effect of longitudinal stresses on wide column buckling. It is conceivable, when the solution will be in hand, that biaxiality will be seen to influence wide column buckling, in which case longitudinal residual stresses would be expected to affect that type of instability and strength.

For general biaxial compressive buckling, use of the solution of Eq. (2) in Eq. (1) yields (for $n = 1$)

$$k_x + (a/mb)^2 k_y = (a/mb + mb/a)^2 \tag{4}$$

where

$$\sigma_{x\,cr} = k_x \pi^2 D/b^2 t \tag{5}$$

$$\sigma_{y\,cr} = k_y \pi^2 D/b^2 t \tag{6}$$

For longitudinal load alone, $k_x = 4$ precisely. For transverse loading alone, $k_y = (1 + 1/9)^2$, or 1.23 approximately.

The theoretical buckling interaction curve for the plates of this project ($a/b = 3$) consists of 3 straight lines as shown in Fig. 1. The coordinates of the transition points are identified on the figure, together with a pictorialization of the buckle mode shape in each zone of the loading combinations. It also follows that the presence of longitudinal stresses due to welding should degrade elastic biaxial buckling stresses.

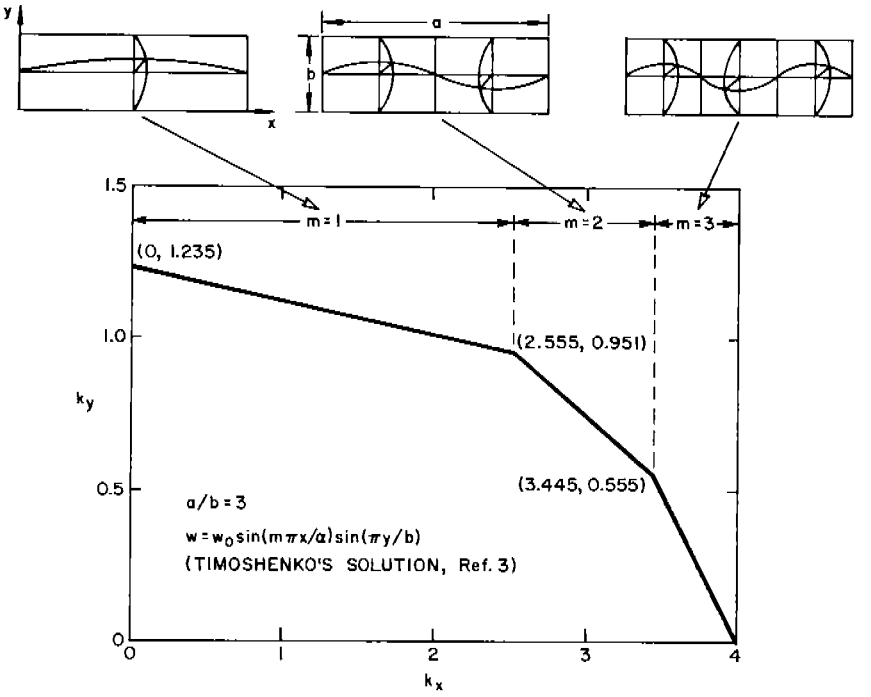

Fig. 1. Biaxial Compression Buckling Interaction Curve for Simply Supported Rectangular Plates

Uniaxial Strength Theories

The ultimate load carrying capacity of a narrow column is essentially the same as the buckling load (Ref. 1). Consequently for uniaxial transverse membrane compression loading, the strength might be expected to agree with the prediction using the classical wide column result of Eq. (6) with $k_y = 1$.

The strength of a plate in uniaxial longitudinal compression was calculated in Ref. 1 using a modification of the two-flange hypotheses advanced by several writers (Refs. 4, 5). The theoretical relation is

$$\sigma_{xu}/\sigma_{cy} = [s/(s+1)][1/s + 2b_e/b + (1 - 2b_e/b)(\sigma_{x\,cr}/\sigma_{cy})] \tag{7}$$

where $$b_e/b = 0.626\,(t/b)(E/\sigma_{cy})^{1/2} \tag{8}$$

and $\sigma_{x\,cr}/\sigma_{cy}$ is found from Fig. 2.

It is seen to fit the scatter band of the older experimental data when s = 8. Through choice of another value for s, the hypothesis can be fitted to the more recent data.

Biaxial Strength Hypotheses

The calculation of the strength of a plate in a general biaxial compression stress field involves recourse to large deflection theory, and consideration of the mode forms as they interact with the different components of the stress field. The hypothesis of multiple flange failure modes represents an attempt to characterize the ultimate load behavior of a biaxially compressed plate in terms of well known phenomena. At present it is an engineering approach of a conceptual nature. The evolution of a rigorous solution must be deferred to a subsequent investigation.

For small b/t, biaxial failure would be expected to occur as plastic buckling involving the entire plate. For that case it may be permissible to use a modified form of the buckling interaction curve. The k_y scale of Fig. 1 may be retained since uniaxial transverse buckling and failure may be synonymous for transverse membrane loads on simply supported plates with a/b = 3.

The horizontal scale was chosen in a somewhat altered form. Instead of enumerating the buckling coefficient for N_x, the ultimate load ratio was used and as a result the abscissa scale of Fig. 1 is shown divided by 4 in Fig. 3. The ultimate load ratio is equal to the quotient of the longitudinal strength under biaxial loading to the longitudinal strength under uniaxial loading. This may be expressed as σ_x/σ_{xu}. It is the same as $(\sigma_x/\sigma_{cy})/(\sigma_{xu}/\sigma_{cy})$. It is also the same as the ultimate force ratio for each tube.

For relatively small b/t both buckling and failure should occur in the plastic range with little difference between them. Consequently the above hypothesis should be applicable to b/t = 30, and possibly to b/t = 50. For larger b/t, however, a different type of failure hypothesis appears to be required after observation of the experiments. This utilizes the flange concept (Fig. 4) which was employed above to predict uniaxial longitudinal strength.

The general ridge line hypothesis of biaxial strength is actually a description of the postbuckling large deflection behavior of the biaxially loaded plate. The hypothesis declares that at low load levels the longitudinal and transverse stresses induce buckles which are comprised of a transverse half wave and one or more longitudinal half waves. This results in transverse ridge lines at the nodes of the longitudinal waves. In plates with b/t large enough to develop the ridge lines, the ridges become the hinge lines for equivalent transverse flanges that carry transverse loads beyond buckling up to the ultimate.

If the plate were initially flat and residual-free, then the buckle waveform in a plate should be developed in accordance with Fig. 1. In the presence of residuals (and also initial imperfections, possibly) the buckle waveform may differ from the configuration in Fig. 1 for a given biaxial field. The effect of an initial imperfection may be large

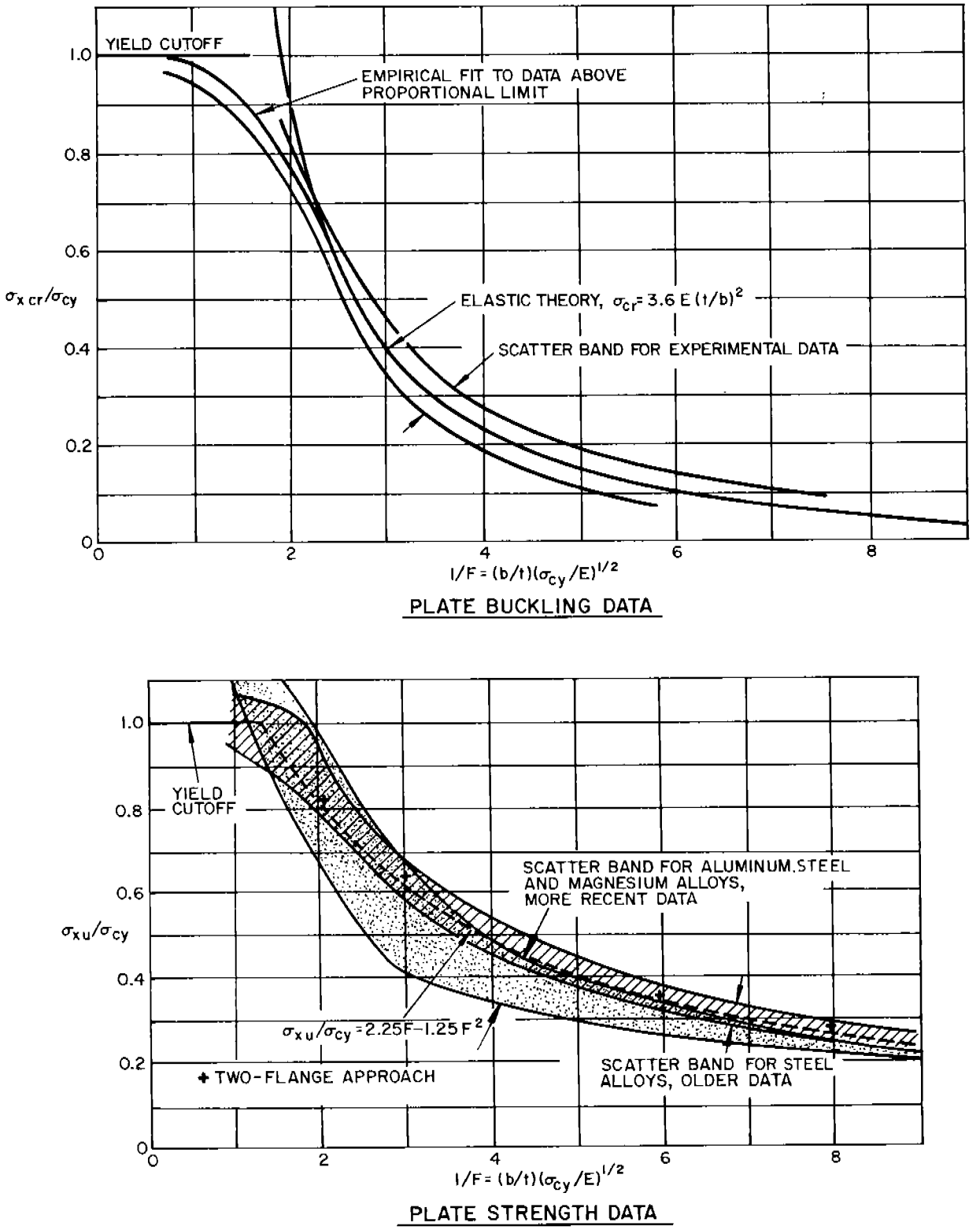

Fig. 2. Buckling and Strength of Longitudinally Compressed Rectangular Flat Plates

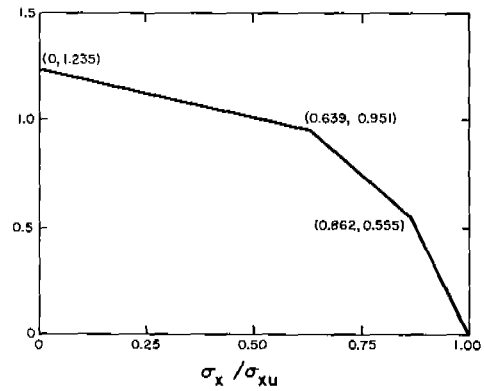

Fig. 3. Hypothesis for Biaxial Strength of Simply Supported Rectangular Plates with a/b = 3

for transverse or biaxial loading compared to longitudinal loading. An imperfection of the order of t/100 may not be directly apparent to the eye, but it could affect the pattern in a biaxial field somewhat in the manner of a corresponding imperfection in a cylinder. The influence of initial imperfections is a subject for further study. Nevertheless, the effects undoubtedly have appeared in the current experiments.

If a plate is loaded to buckling in biaxial compression, then the buckle form may take any of the three shown on Fig. 1, providing a/b = 3. This could induce ridge lines across the plate at the node points. In fact, if a transverse stiffener were to be present, the ridge lines would be enforced even though b/t were to be less than 3, and the plate buckling stress could be computed in the same manner as above except that now the effective a/b of the plate might be altered.

Suppose that each ridge line acts as an invisible stiffener. Then the material on each side of the ridge would behave in the same manner as a flange. This situation is depicted in Fig. 4. Failure of the plate would be expected when flange failure occurs on either side of each ridgeline. From this hypothesis the plate ultimate load can be computed if the failure stress is selected at the yield level, and the relation for the buckling stress of a flange is utilized. The expression would be

$$\sigma_{cy} = \eta k_y \frac{\pi^2}{12(1-\nu^2)} E(t/b_e)^2 \qquad (9)$$

in which the plasticity reduction factor, η, would be equal to E_s/E for a long hinged flange. In the case of the mild steel used for the current investigations, failure may be assumed (tentatively) to occur at yield and no plasticity reduction need be considered. Consequently, since all the quantities in Eq. (9) are known except the effective width of the flange for a given k_y, then

$$b_e/t = 0.63(k_y E/\sigma_{cy})^{1/2} \qquad (10)$$

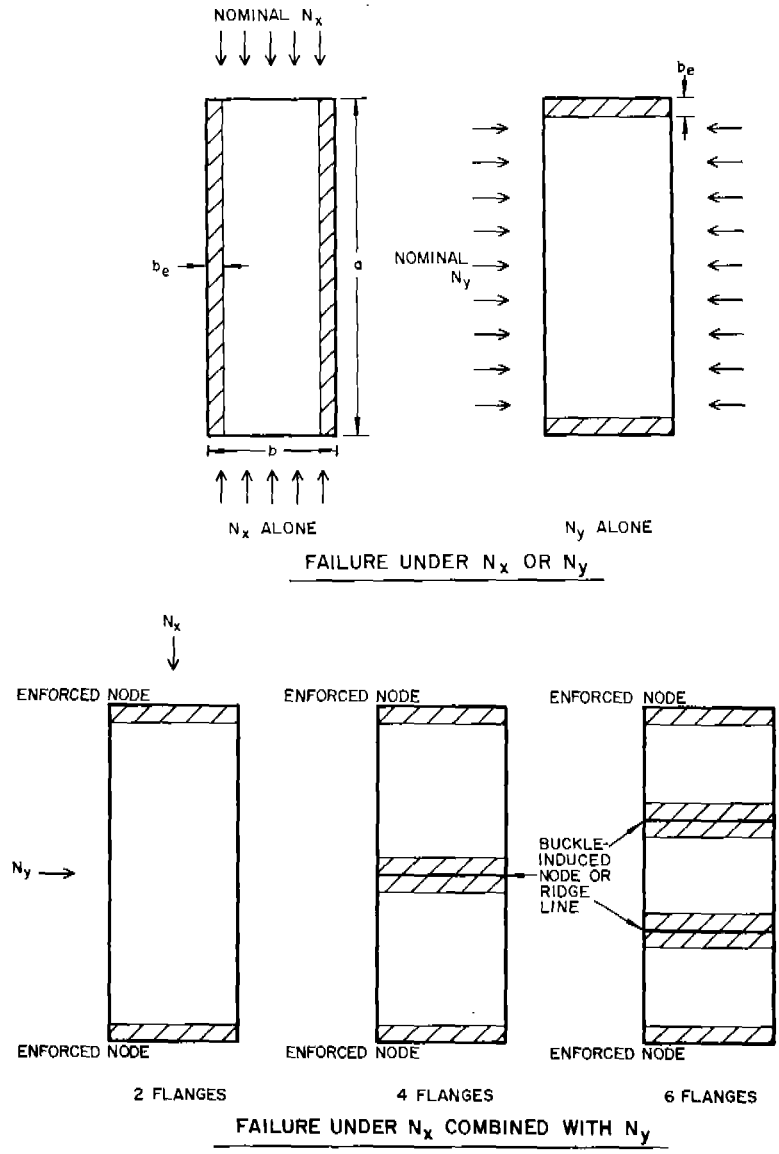

Fig. 4. Equivalent Flange Concepts for Rectangular Plates

For a long flange (b_e considerably less than the flange length) $k_y = 0.433$. However, for shorter flanges the value of k_y depends upon the flange length. Since the length of the transverse flange is the plate width, b, then it is only necessary to determine the relation of k_y to b_e/b. For selected values of b_e/b Timoshenko provides data on this relation for hinged as well as clamped flanges (Ref. 3). The determination of the effective flange width may then be pursued in an iterative fashion from those data. Fig. 5 contains the intermediate data and the final desired result for a hinged flange. For the four cases of interest here the theoretical values of flange width and force at yield appear in Table 2.

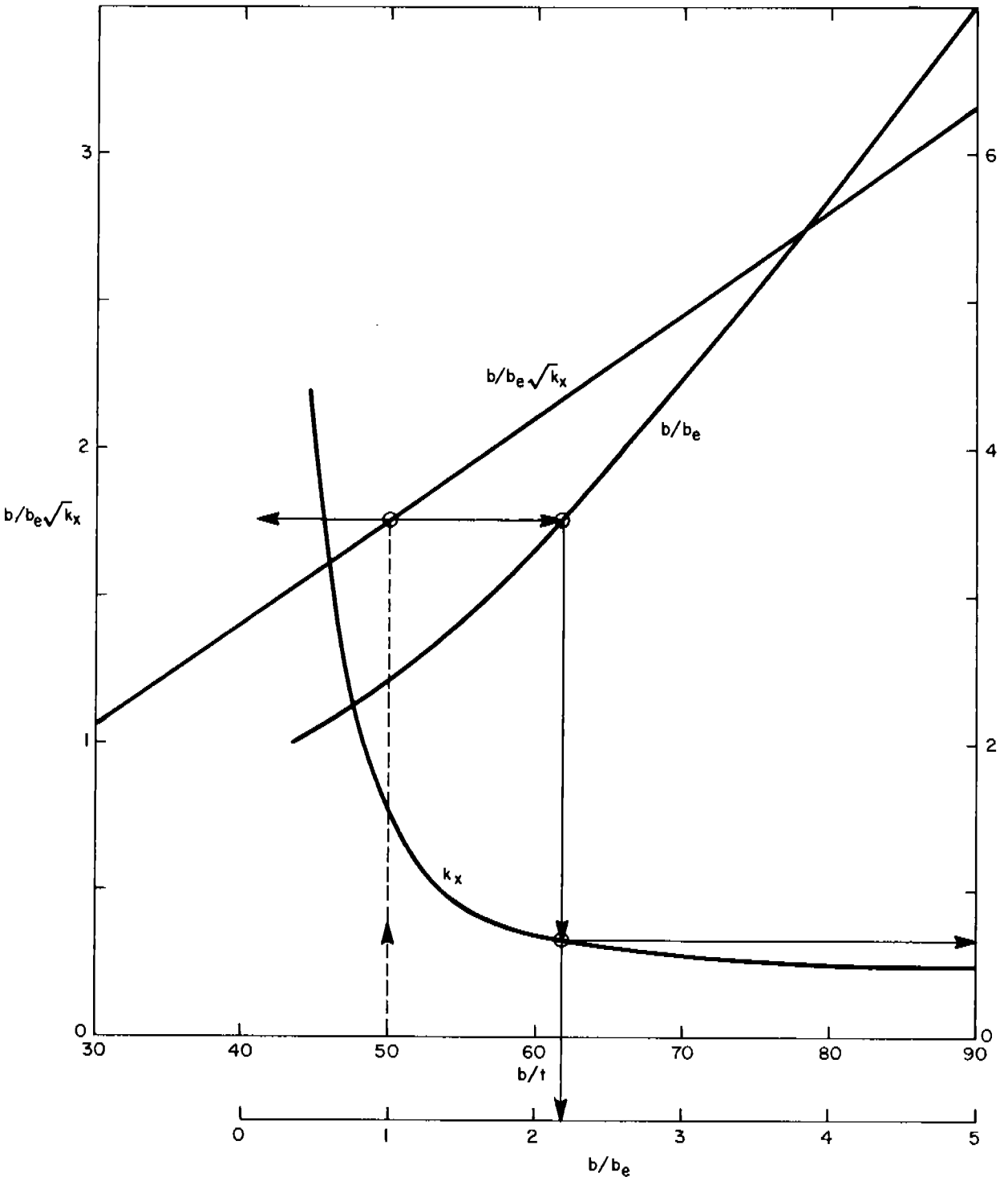

Fig. 5. Effective Widths and Buckling Coefficients for Equivalent Hinged Flanges

Table II. Effective Flange Dimensions and Forces

b/t	30	50	70	90
b (in.)	0.90	1.50	2.10	2.70
b_e (in.)	1.64	0.70	0.63	0.61
P_2*(10^3 lb)	---	1.65	1.48	1.43

*Load per flange pair, $39{,}200 \times 0.03\, b_e$ since $\sigma_{cy} = 39.2$ ksi

If a three lobe buckle should occur, then there would be a distance equal to b between each pair of ridgelines. Obviously, since one flange would lie on each side of the ridgeline within each lobar region (Fig. 4) then at b/t = 30 the two effective flange widths would exceed the plate width. Furthermore, for b/t = 50 these dimensions would be almost the same. Therefore the usefulness of the flange hypothesis for those cases may be doubtful or borderline. Failure would be expected to occur more in the manner of plate plastic buckling. However, for larger b/t there appears to be a possibility that the flange hypothesis could be helpful in explaining the observed experimental data.

In the preceding the flange was assumed to be hinged. This appears to be a reasonable assumption for interior ridgelines. For the two loaded edges of the plate, however, there may be some question as to the exact nature of the flange boundary condition during tests. The discussion of this factor appears in the section on biaxial strength.

Influence of Residual Stresses

Introductory Comments

The ultimate strength of a longitudinally compressed plate has been treated theoretically as though the postbuckling configuration of the plate is representable either as a pair of flanges hinged along the plate edges for plates which buckle long before failure (large b/t), or as a plate which buckles plastically as a whole (small b/t). In either case the strength of the plate is computed as though the failure process were a form of plastic buckling. Therefore, if the influence of residual stress upon plate buckling can be established in the elastic or inelastic range, it is hypothesized that the influence may be applied to plate strength also. This hypothesis is not rigorous. It is offered as a means of explaining the observations of this investigation and of correlating the experimental data on the influence of residuals.

The influence of residual stresses on uniaxial compressive strength may be determined with the aid of two principles of plate instability:

1. After a plate buckles, the critical load is sustained across the plate while any additional load is supported mainly by two flange-like strips along the unloaded edges. This pertains to plates which have critical stresses considerably below yield.

2. For plates which buckle elastically or inelastically, the determination of the critical stress may be accomplished by computing the critical strain and then entering a suitable stress-strain curve to determine the critical stress.

The first principle is generally well-known. It is discussed in Ref. 1, for example. The second principle was employed successfully by Gerard (Ref. 6) to demonstrate that the proper plasticity reduction factor for a hinged flange is E_s/E.

In the following, use is made of these principles to calculate the influence of residual stresses on plate strength and to show that the influence diminishes to a negligibly small amount as b/t becomes small.

Outline of Procedure

The important features of the calculation scheme are depicted schematically in Fig. 6. An appropriate stress-strain curve appears at the top in nondimensional form. The modification involves the correction to the curve to reveal the proper relation between strain and stress when the appropriate plasticity reduction factor is taken into account. For a flange no modification is necessary since the secant modulus governs. For a simply supported plate, however, (Ref. 1)

$$\eta = \frac{1 - \nu_e^2}{1 - \nu^2} (E_s/E) \left[(1/2) + (1/4)(1 + 3E_t/E_s)^{1/2}\right]$$

and consequently the relation would have to be changed to reflect this more complex expression. Actually, if the experimental data of Fig. 2 are employed, then the modified curve will reflect this more suitable relation between strain and buckling stress. That has been done in Fig. 6.

The trend of $\sigma_{x\,cr}/\sigma_{cy}$ is shown as a function of b/t in Fig. 6. together with the appropriate stress-strain curve. The critical strain ratio is

$$\epsilon_{x\,cr}/\epsilon_{cy} = 3.62(t/b)^2/\epsilon_{cy} \qquad (11)$$

utilizing an elastic-plastic stress-strain curve so that $\epsilon_y = \sigma_{cy}/E$.

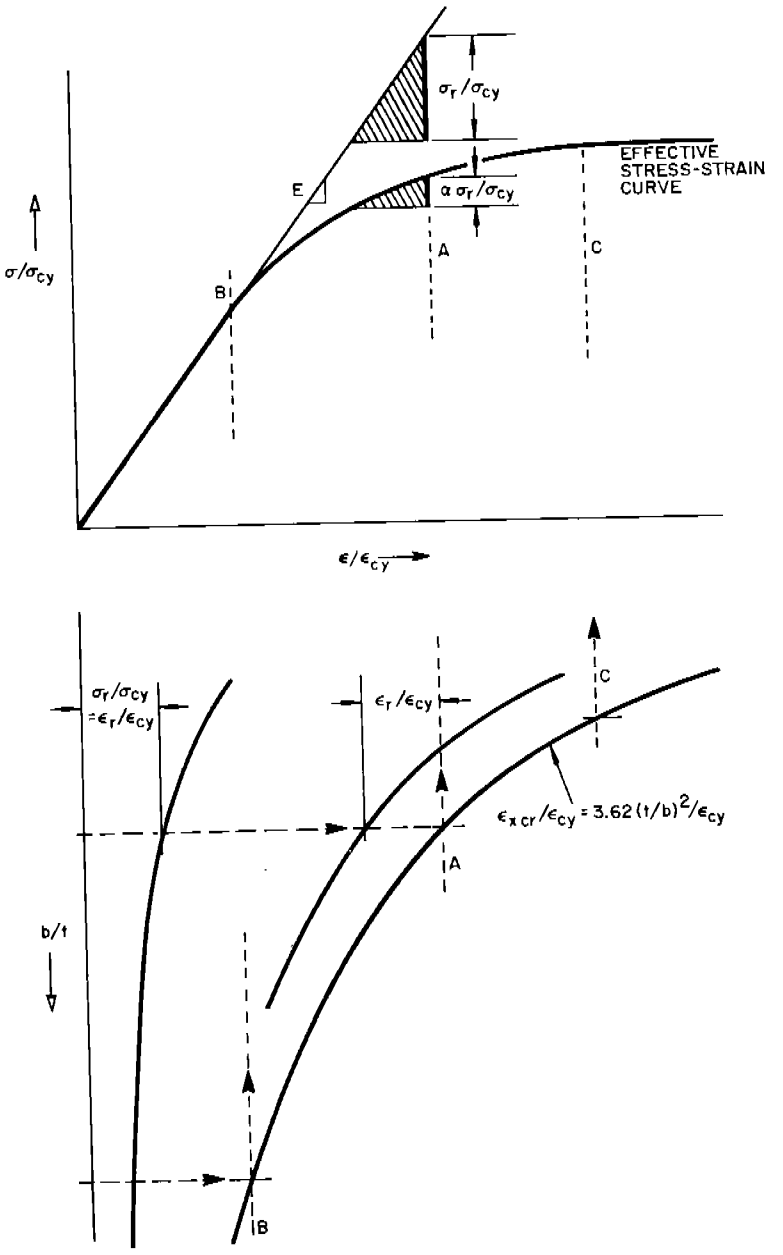

Fig. 6. Determination of Effective Residual Stresses

Eq. (12) comes from the expression in Eq. (8) for the elastic compressive buckling stress of a simply supported flat plate

$$\sigma_{x\,cr} = k\,\frac{\pi^2 E}{12(1-\nu^2)}\,(t/b)^2 \qquad (12)$$

where k = 4 and Poisson's ratio = 0.28 for mild steel. The critical strain is obtained by transposing E to the bottom of the left side of Eq. (12). The remaining quantity on the right becomes the critical strain. The elastic portion of the $\epsilon_{xcr}/\epsilon_{cy}$ function may be extended

as a high as required to permit completing the construction of the effective residual stress relation.

The residual strain ratio is simply σ_r/σ_{cy} since Young's modulus cancels top and bottom.

The bottom of Fig. 6 contains plots of ϵ_r/ϵ_{cy} and $\epsilon_{x\,cr}/\epsilon_{cy}$ as a function of b/t, which increases downward in the figure. The two curves on the right are the critical line, and the critical line reduced by the residual. Both nondimensional strain plots and the modified stress-strain curve in nondimensional form are used in evaluating the influence of residual stress on strength. The process is depicted for elastic values of σ_r and $\sigma_{x\,cr}$. Enter the lower diagram at a selected b/t and identify the corresponding ϵ_r/ϵ_{cy} and $\epsilon_{x\,cr}/\epsilon_{cy}$, as at A. Rise to the modified stress-strain curve and read the effective σ_r/σ_{cy}. It is apparent that when σ_r/σ_{cy} occurs at B the limit of unity for a will have been reached. At C and above the value of a approaches zero. Between these two positions on the σ_r curve a undergoes a rapid degradation. Therefore, the general relation

$$a\sigma_r/\sigma_{cy} + \sigma_x/\sigma_{cy} = \sigma_{xu}/\sigma_{cy} \qquad (13)$$

would be applicable. The transition of a from 1 to 0 as b/t is decreased reflects the role of plasticity in controlling the influence of residual stress on strength.

Effect of Normal Pressure

A detailed discussion of the effect of normal pressure appears in Ref. 1. That discussion included an examination of the nature of the load increase by the conversion of the flat plate to a segment of a cylinder loaded in longitudinal compression.

According to the theoretical predictions of Levy and his colleagues, (Ref. 7), a significant (even a very large) increase in buckling load would be expected for large lateral pressures. However, when the effect of initial imperfections in cylindrical shells is taken into account, the anticipated increase may be so small as to be negligible, or only a few percent at most.

The significance of this information to the effect of pressure on hull plates may be summarized in the conjecture that an inappreciable gain would be anticipated in the buckling or maximum load carrying capacity of a longitudinally compressed plate as the result of the application of normal pressure.

When a plate is loaded simultaneously by normal pressure and transverse membrane compression, the effect of the normal pressure would be to produce an initial imperfection, similar to a slightly prebent column. Timoshenko has shown (Ref. 3) that such an initial load would have a degrading effect upon the strength of the column and

could degrade it considerably when large normal pressures are applied. Consequently, it is conceivable that under the combined action of normal pressure and transverse membrane compression, both transverse and biaxial strengths of a plate may be degraded much more than under longitudinal compression alone. A preliminary examination of this effect was made by attempting to adapt Timoshenko's data for slightly bent columns (Ref. 3). However, the predictions were not close to the observations and the study was halted. This area warrants further pursuit in subsequent studies.

Theories of Yielding

For some cases of loading, plate instability may be controlled by material yielding. Two yielding theories (see Ref. 8, for example) are in general use depending upon the nature of the material and the type of problem being investigated. The maximum shear theory requires that the largest algebraic difference in principal stresses is equal to the yield

$$\sigma_{cy} = \sigma_x - \sigma_y,\ \sigma_y - \sigma_z,\ \text{or}\ \sigma_z - \sigma_x \tag{14}$$

whichever is greatest, while the octahedral shear theory requires that

$$2\sigma_{cy}^2 = (\sigma_x - \sigma_y)^2 + (\sigma_y - \sigma_z)^2 + (\sigma_z - \sigma_x)^2 \tag{15}$$

There is little difference between them as may be seen in Fig. 7 for the plane stress case ($\sigma_z = 0$) when σ_x and σ_y are of the same algebraic sign as in the current investigation.

Use will be made of these theories in evaluating biaxial strength data.

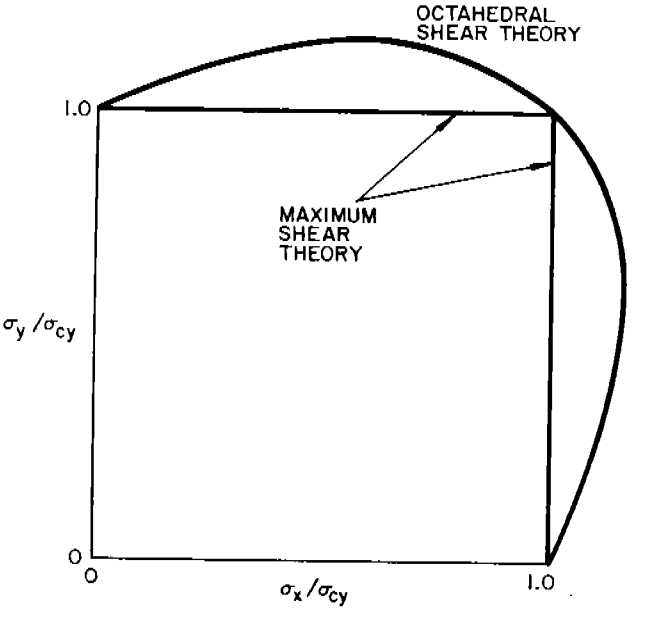

Fig. 7. Plane Strength Theories

SPECIMEN CHARACTERISTICS

Shapes and Dimensions

All strength test specimens were square cross section tubes fabricated from flat rectangular plates by the use of electron beam welding along the four edges. The details of the welding appear in the section, Residual Stresses. The material was nominally 0.030 inch thick. Fig. 8 depicts the specimens and shows the dimension ranges.

Material Properties

All test specimens were fabricated from readily available sheet steel stock. The material was 22 GA. 0.0299 inch nominal thickness AISI No. 1020, commercial quality, cold rolled steel received in 3 foot by 8 foot sheets. All the sheets were part of the same mill run, insuring uniformity of composition and properties within reasonable limitations.

The 3 × 8 sheets were sheared into 2 foot by 2 foot and 1 foot by 2 foot sections. Each section was marked to identify the 3 × 8 from which it had been cut. The sections were then process-annealed at 1200°F in an inert gas atmosphere and oven-cooled.

Additional samples were cut from the parent plate and were subjected to another annealing cycle along with 4 tube samples in order to remove residual stresses.

Tension and compression stress-strain tests were performed to identify Young's modulus. Poisson's ratio, and the yield strength. The results are shown in Table 3.

The elastic tension stress-strain curve was obtained by a point-to-point loading process using back-to-back strain gages to obtain a reference value for Young's modulus. It is evident in Table 3 that this was in the range of the usual value, and agreed well with the compression E values. They were secured in a buckle-preventing compression jig employing strain gage pairs as shown in Fig. 9. It is interesting that the E values from Dwight and Ractliffe's load shortening data were 5/6 the usual value of 29 to 30 msi., which they employed in calculating F for the steel specimens.

Effective Stress-Strain Curve

The shape of the compressive stress-strain curve was difficult to obtain in the yield region for the material from which the specimens of this investigation were fabricated. This arose from the tendency for the specimen strips to buckle at a stress close to yield. The buckles were of extremely short wavelength, as would be expected for

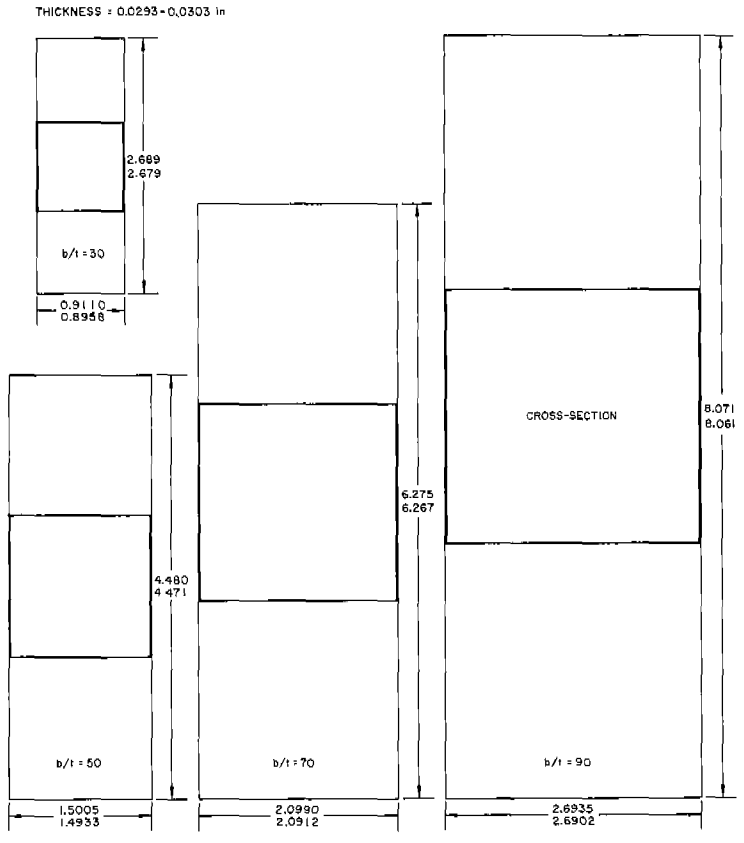

Fig. 8. Specimen Dimensions Showing Maxima and Minima on Sketches of Tubes

Table 3. Material Properties Tests

Test Type	Specimen Type	σ_{cy} ksi	E msi	ν
C	Sheet	38.5	29.0	
C	Sheet	39.4		
C	Sheet	39.2		
C	Sheet	39.6		
C	Sheet	38.6		
C	Sheet	39.4		
C	b/t = 15, box	40.0		
C	b/t = 30, box			.274
C	b/t = 50, box			.289
C	b/t = 70, box			.282
C	b/t = 90, box			.280
		39.2 av		0.28 av
T	Sheet	40.5	29.0	
C	Sheet*	39.0		
C	Sheet*	38.2		
C	Sheet*	41.2		

C - Compression T - Tension

* Reannealed Specimens

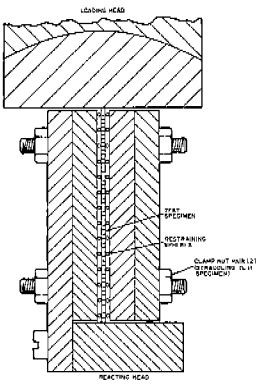

Fig. 9. Sheet Compression Test Jig

a material with a tangent modulus approaching zero and which exhibits Luders bands. Actually, at strains beyond yield the tangent modulus was found to have a value of 0.8 msi. For practical purposes, however, the material was essentially elastic-plastic. It approached the schematic form shown in Fig. 10, but with a sharper knee.

For calculation of plastic buckling stresses, the curve of Fig. 2 should be employed. If the strains which relate to each value of b/t are plotted against the corresponding $\sigma_{x\ cr}/\sigma_{cy}$ value, then an effective stress-strain curve may be constructed for the model material. This has been done in Fig. 10 by making use of the relation

$$\epsilon_{x\ cr} = \sigma_{x\ cr}/E = 3.62(t/b)^2 \qquad (16)$$

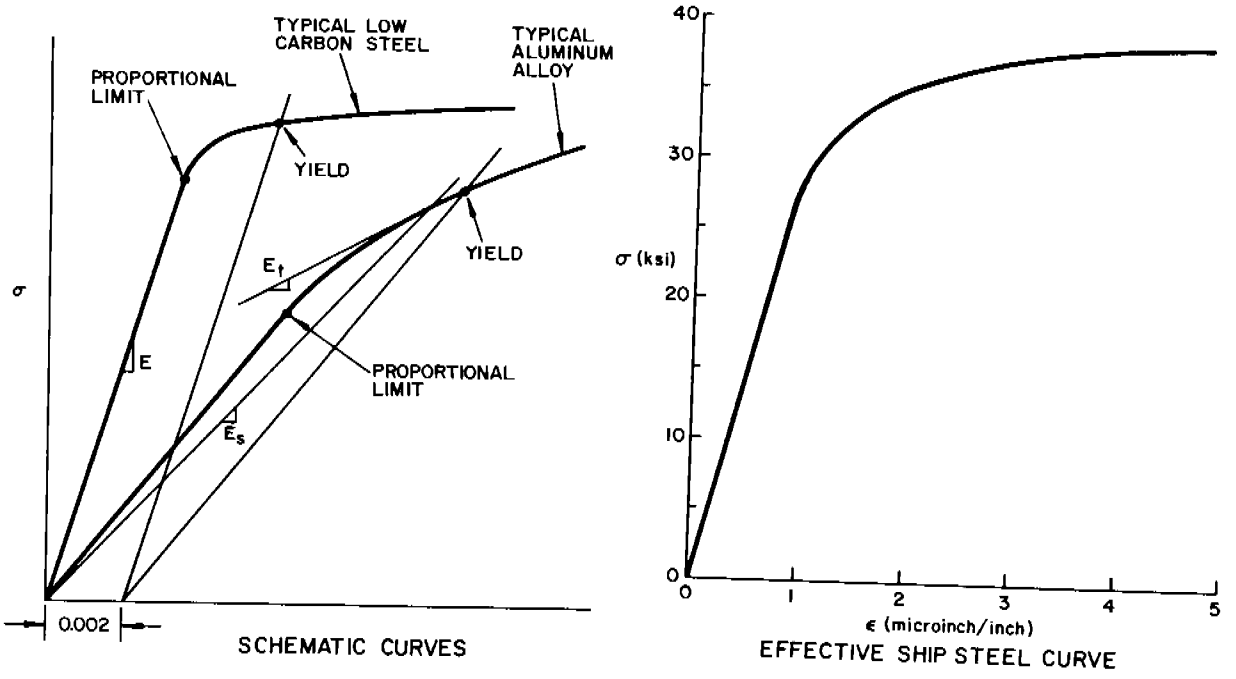

Fig. 10. Stress-Strain Curves

LOAD APPLICATION DEVICES

Equipment

The unstiffened plate experiments involved the application of a variety of load types to square cross section sheet metal tubes, each with a length equal to three times the dimension of a side of the square. The problem was to apply the forces uniformly along each loaded surface with no frictional resistance to Poisson ratio strain tendencies, and in a manner that would meet the boundary conditions stipulated for the tests.

Two testing machines and several fixtures were employed to accomplish the project goals. The large loads were applied by a three-column testing machine of unique manufacture, capable of applying 25,000 pounds of force through pneumatically actuated bellows much in the manner of a deadweight load applicator (Fig. 11). The smaller loads were generated by a two-column pneumatic machine with 4,000 pounds capacity (Fig. 11). The pressurization systems for both machines incorporate load balancing features which provide great stability of the applied load at any level.

Fixtures for transverse load application to the tubes are shown in Fig. 12, which also displays the lateral support device for compression material property tests of thin sheet. A schematic of the transverse loading system appears in Fig. 13.

The load scale on the dial gage face of the large machine is graduated in 20 pound increments with reliable interpolation to 10 pounds. On the small machine these values are 2 pounds and 1 pound respectively. Both machines were calibrated frequently during the project, although the load precision for each is minuscule compared to the size of the scatter in the experimental data.

Both testing machines are employable in the same manner as all other standard machines. The most significant departure is the use of three columns on the large machine which imparts a greater measure of stability during the conduct of a test on a slender compression specimen. This property of the machine would have the virtue of minimizing possible variations of load distributions which could occur during similar tests on conventional machines. The smaller machine was employed for loads which did not require this type of stability and, therefore, was adequate for the purposes of this investigation.

The details of the uses of the machines and fixtures are included in the following discussions on the types of tests conducted on the tubes.

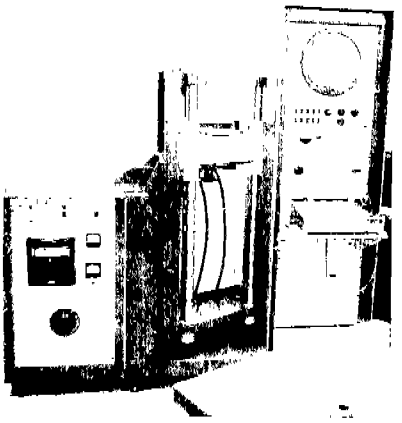

a. 25,000 pounds

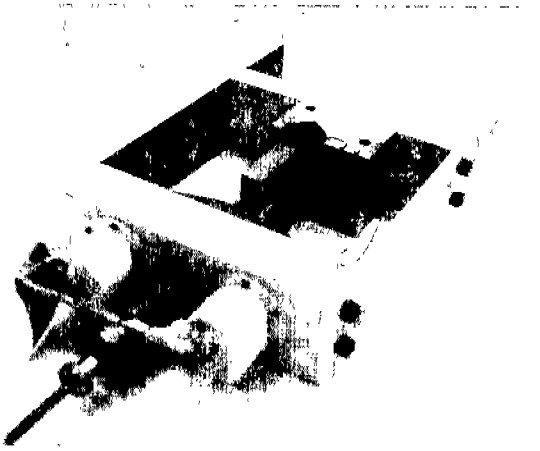

b. 4000 pounds showing transverse compression fixture in place.

Fig. 11. Testing Machines

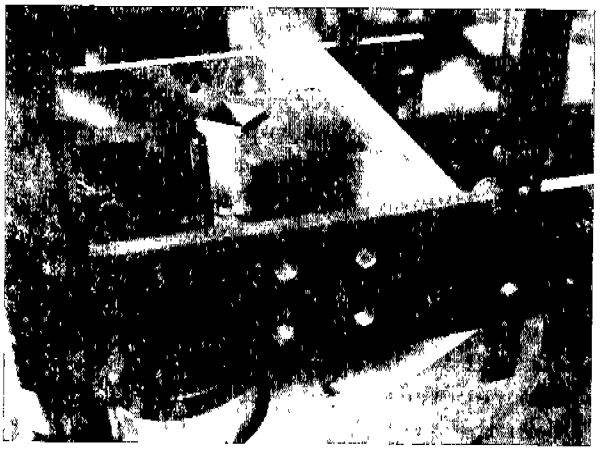

a. transverse compression fixture

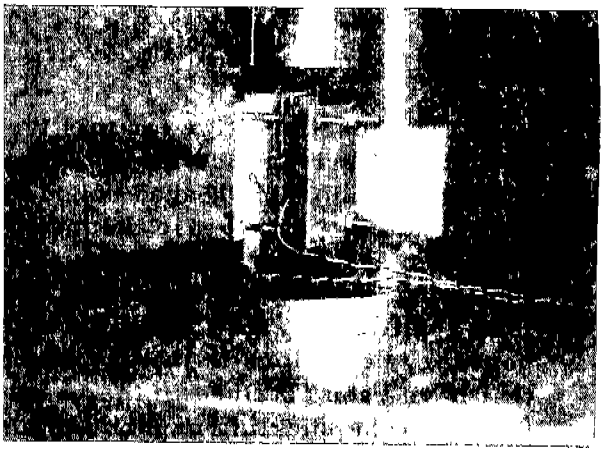

b. stabilization of sheet during compression property tests

Fig. 12. Closeups of Fixtures

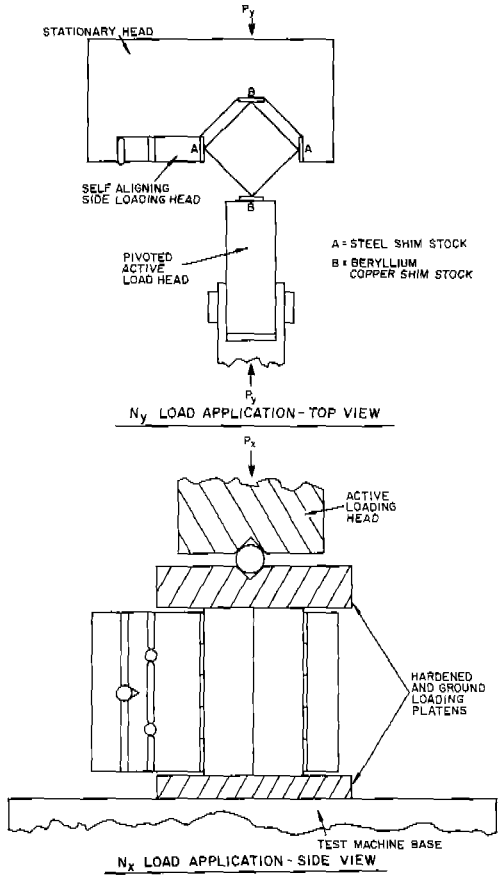

Fig. 13. Schematic of Transverse Compression Fixture

Uniaxial Compression

The test condition for this type of loading (N_x) was the application of a compressive force along the longitudinal axis of symmetry of each tube while enforcing hinged boundary conditions along the loaded edges of the plates. It was also theoretically important to permit freedom of movement in the y direction along the loaded edges so as to avoid inhibiting the Poisson expansion which would accompany the longitudinal load application. The basis for accepting the existence of the above boundary conditions is the agreement of instability data for long plates that have been obtained in the past, and which receives some substantiation in the buckling experiment described in the section, Uniaxial Compression. No direct test was conducted to determine whether the conditions actually were met during these experiments. However, the reason for confining the current tests to $a/b = 3$ was the belief that deviations from the specified boundary conditions would not influence the data significantly. The restraint of movement normal to the plane of the plate may be assumed to be reasonably well met by the frictional forces under the loading head. Rotational and Poisson effects presumably would not be important because of three-lobe buckle patterns to be expected in the plates and the knowledge that a small amount of rotational restraint would not tend to increase the buckling stress significantly. Some measure of support for this point may be gained from Fig. 14 which reveals only about 7 percent increase in the buckling

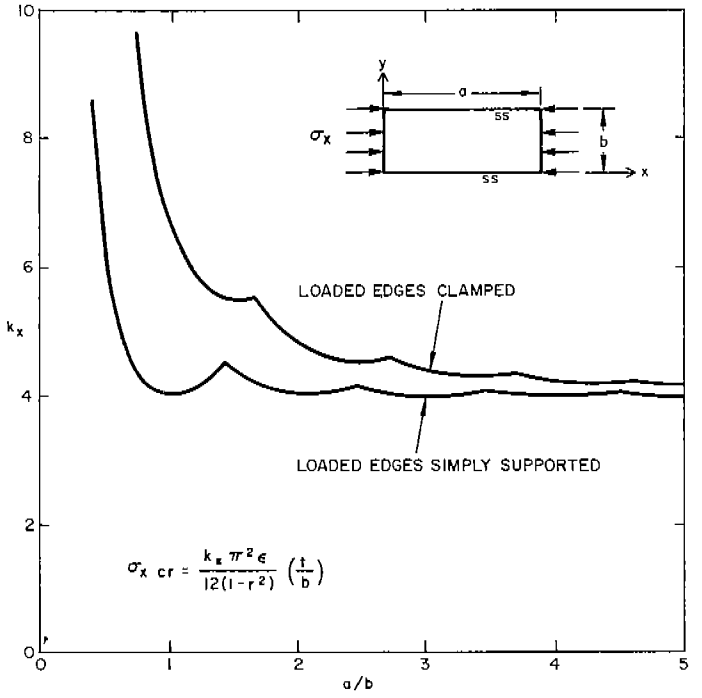

Fig. 14. Buckling Data for Plates

stress of a plate for a/b = 3 when the loaded edges are fully clamped. The realization of full rotational restraint at the unloaded edges is highly unlikely, however, which reduces the potential gain in plate strength to a few percent at most.

Uniformity of longitudinal loading along the edges of the tube cross section is generally possible only when the edges are polished flat to within the order of 0.0001 inches or less. In addition, all four loaded edges of a tube must lie in a plane to within the same order of tolerance. Finally, the lateral displacement of the load axis cannot deviate more than 0.001 inches from the tube axis to avoid inducing significant bending moments along the tube length, thereby minimizing load distribution variations across the square section of the tube. All these criteria appeared to have been satisfied by the careful manufacture of the tubes.

Biaxial Compression

The application of biaxial compression required the development of a feasible loading concept followed by construction of fixtures which would permit the effective implementation of that concept. Furthermore, the criteria for effective longitudinal load application still applied, multiplied in complexity by the same general requirements for the transverse loading, and finally complicated by the requirements for successful simultaneous load application.

The two most difficult problems were the achievement of uniform transverse loading along the length of the tube in spite of the varying tube cross section dimensions induced by Poisson strains which were partially restrained along the longitudinally loaded faces but which were

unrestrained in the middle of each tube, and by the need for avoiding frictional resistance to the longitudinal and transverse motions of the transversely loaded edges of the tube. These features were attained with reasonably good success through the use of the fixtures depicted in Fig. 12 and sketched in Fig. 13. Data on the degree of uniformity and proper values of the transverse and longitudinal loads were obtained by extensive strain gaging to measure the distributions up to 90 percent of failure in biaxial tests.

The fixture configuration was the final result of preliminary tests with other concepts that failed to meet the above criteria satisfactorily. The present fixture still does not eliminate friction completely. Further effort may be required before it could be reduced to a small fraction of one percent of the transverse loading. Nevertheless, on the basis of the strain gage data obtained during the tests the current fixture was judged satisfactory for the purposes of the project.

The wide column tests required only the small loading machine with no forces applied to the specimen ends. The attempts to achieve simple support at the tube ends in order to perform transverse load tests on plates with all edges hinged were unsuccessful unless a small longitudinal force were applied to the specimen. In addition, the use of cement to aid the acquisition of simple support on the short edges of the plate appeared to help. Both of these latter steps were taken in a few experiments in which a small axial load was induced by the application of a small internal vacuum to the specimen. The resultant axial stress was of the order of 1 percent of the longitudinal strength.

Pressure Tests

Both internal vacuum and positive internal pressure applications were possible with the use of the perforations and tubing in the upper loading platen through which longitudinal compression from the testing machine passed into the specimen. Sketches of the vacuum and positive arrangements appear in Fig. 15. Vacuum pressure was read with a mercury monometer while positive pressure was measured with a standard dial gage. These both permitted direct reading to 0.1 psi. Interpolation to 0.05 psi was possible. The bleed control for the pressurization system provided the same degree of load stability as in the testing machines.

Material Property Tests

The determination of Young's modulus, Poisson's ratio and the yield strength were accomplished in a variety of ways. The compression properties were measured by longitudinal compression tests on a square tube manufactured to $b/t = 15$, and $a/b = 6$, using the 0.030 inch thick sheet from which the test specimens were made. In addition, single plates were compressed longitudinally in the stabilization jig shown in Fig. 9. The tension tests were conducted in the usual manner in the jaws of the small machine. Direct measurement of Poisson's ratio was accomplished during the performance of the wide column tests by employment of suitable strain gages described below.

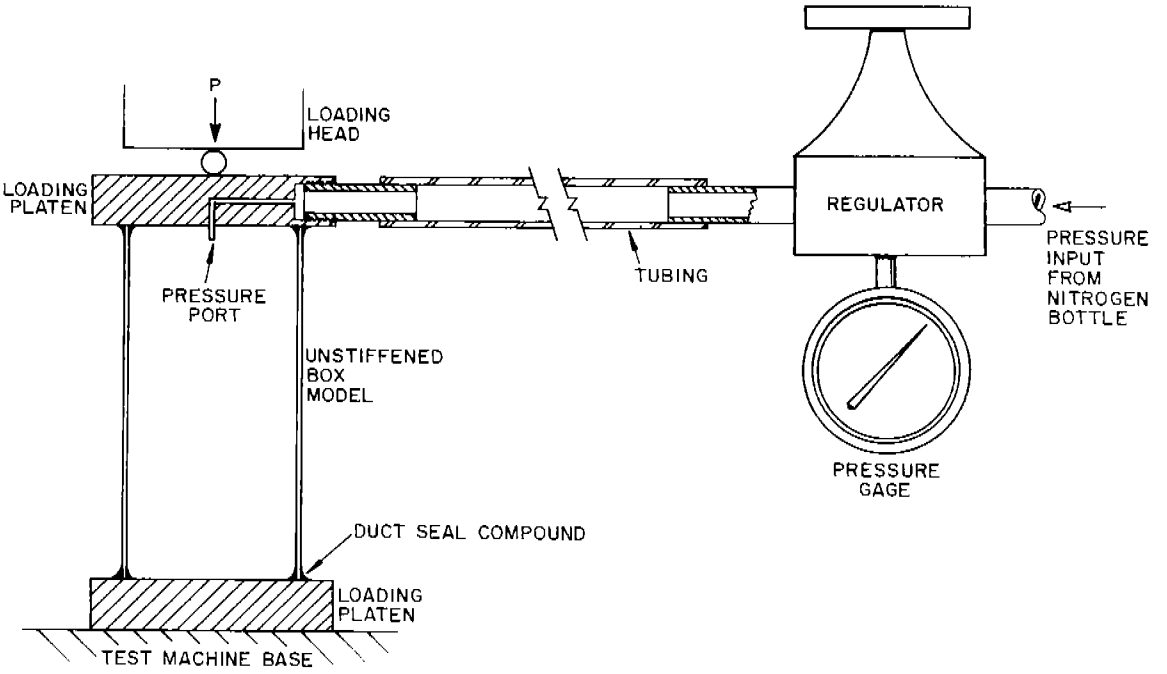

MODEL TEST WITH INTERNAL PRESSURE

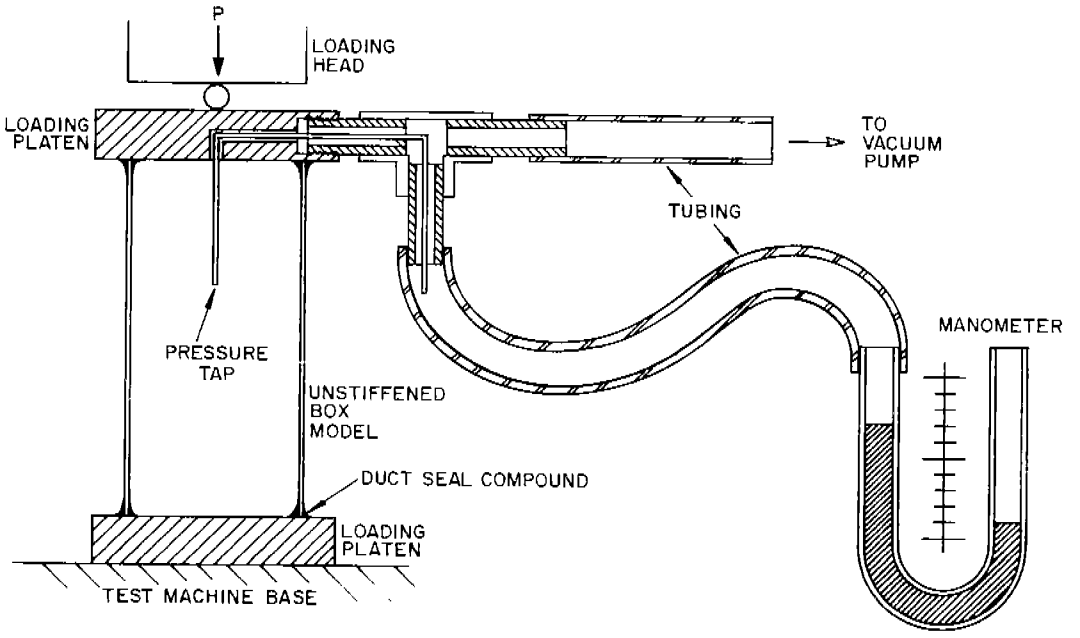

MODEL TESTS WITH INTERNAL VACUUM

Fig. 15. Sketches of Pressurization Systems

DATA ACQUISITION

Load

The magnitudes of the applied loads were measured with the calibrated dial gages on the testing machines. Through employment of the load rate controllers it was possible to apply the longitudinal and transverse forces at virtually any rate from static to near-impact. Most longitudinal compression tests were conducted with a load application rate of 1,000 pounds per minute. The transverse loads were applied point-by-point. However, when load combinations were applied to tubes, one of the components was held static while the other was varied throughout a preselected range.

Data on load and time were recorded on a Mosley X-Y recorder. In many cases a stopwatch aided manual control of the longitudinal load rate. A typical record is reproduced in Fig. 16. The scales are readable to a precision of 10 pounds in load and 5 microinch/inch in strain. This compares well with the dial gage precisions of 20 pounds and 2 pounds for the large and small testing machines, respectively.

Pressure

The pressures which were applied to the interiors of the tubes (either positive or vacuum) were measured by a tap placed in the line so that the pressure in the specimen interior could be read directly. This is preferable to reading the inlet pressure, which procedure is subject to errors when the pressurization gas is flowing because of the dynamic head.

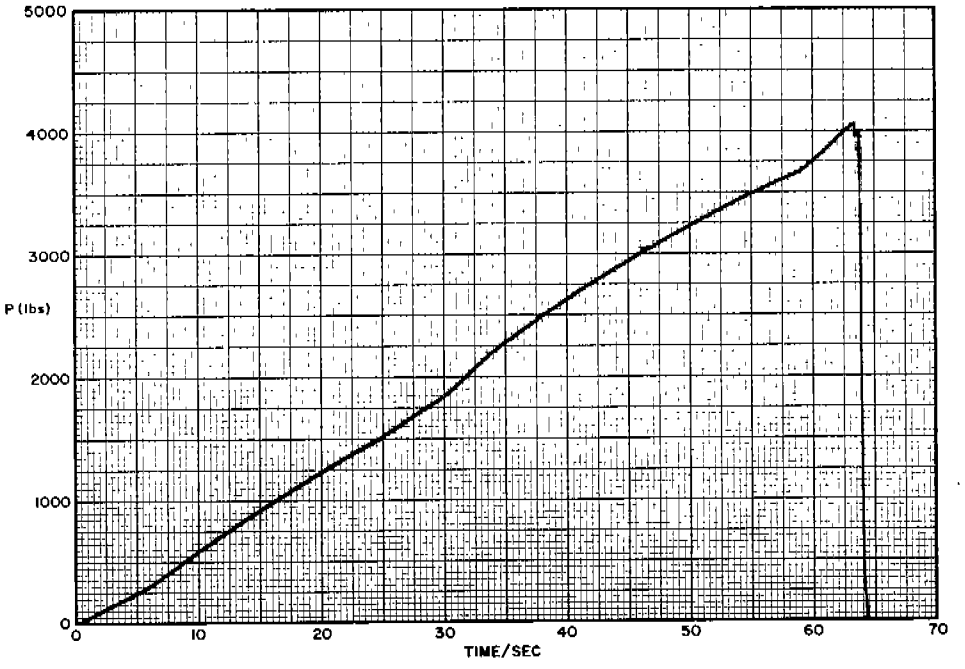

Fig. 16. Typical Load-Time Trace

Strain

Strain data were obtained with bonded electric strain gages which were read directly to 5 microinch/inch with interpolation to 1 microinch/inch, using a BLH Strain Indicator Model 120 C. The gages varied in size and characteristics. The range of properties is listed in Table 4.

Table 4. Strain Gages

Gage Type	Resistance ohms	Gage Factor	Transverse Correction	Gage Length in.	b/t
FAE-50-1256	120	2.05	-0.2%	.50	90 70
FAE-12-1256	120	2.01	+0.3%	.125	50 30

They were used to obtain stress-strain data, residual stresses, membrane stresses during biaxial loading, the onset of instability in two buckling experiments, and a variety of preliminary data obtained during the early stages of the investigation to maximize the efficiency with which the project was prosecuted. No data from the preliminary studies are reported, however, because of the lack of relation to the project.

All strain gages were mounted on the sheet material in back-to-back arrangement (Fig. 17). In some cases the outputs were summed to obtain mean membrane strains while other tests (the buckling experiment, for example) utilized the strain differences to obtain bending curvatures. At some locations the gages were aligned longitudinally only, as in the stress-strain tests. In others right angle pairs were used where the Poisson strains were required to permit calculation of the two components of the biaxial membrane stress field. Because of the large number of tests performed in this investigation a minimum number of gages was employed on each specimen in order to obtain the pertinent data in minimum time, and also at minimum cost to the project. In fact, no strain gages were applied to the longitudinal strength specimens since the ultimate load and the cross section area were the principal data required from those tests.

Experimental Errors

The maximum range of specimen dimensions may be seen in Fig. 8. The extreme variation in thickness, from the nominal of 0.030 inches, was 2 percent, but the mass of data yielded a variation of less than 1 percent. The largest deviation from the nominal specimen width (b/t = 30) was 2 percent. All others were of the order of 1/2 percent. Therefore, use of the nominal cross section area (instead of

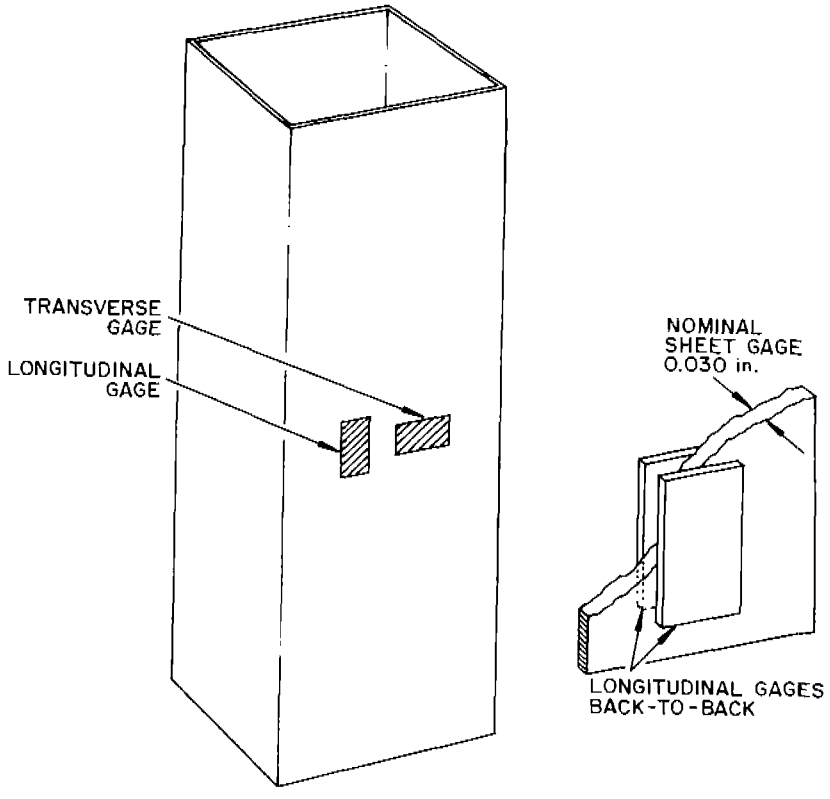

Fig. 17. Strain Gage Application

the directly measured value) could have involved a maximum error of 3 percent for $b/t = 30$ and 1.5 percent for all other specimens. Furthermore, the maximum departure from nominal of the theoretical elastic longitudinal buckling stress could have been 6 percent for $b/t = 30$ but would have been less than 3 percent for b/t greater than 30.

All specimen lengths were smaller than nominal by 1 percent or less, which would have introduced a negligible effect on longitudinal buckling stresses (and probably on strength also) since the buckling coefficient curve is flat at $a/b = 3$. There could be a maximum deviation of 4 percent in the theoretical wide column buckling stress and 2 percent in the applied transverse stress.

The maximum load variation could have been no more than 1/2 percent at the longitudinal compression failure loads, and the same accuracy would apply to the transverse forces. The strain gage data are considered reliable to better than 1 percent.

SUMMARY OF EXPERIMENTAL DATA

Tables 5, 6, and 7 contain the pertinent data acquired during the experiments conducted in this phase of the project on the compressive strength of ship hull girders. The tests in those tables represent approximately half of the total number of experiments which were conducted.

In a sense, each tube test represents the average of four tests. The use of tubes hypothetically guarantees simple support along the long edges of each tube and therefore permits a set of four simultaneous tests on four plates nearly identical in geometry and material properties. The uniformity of geometry throughout all the tubes is shown in a preceding section of this report. If the loaded edges of the cross section are flat so that uniform load can be applied to all four face plates of each tube, then the slight readjustments which would occur in the stress distribution at loads near failure would tend to emphasize that uniformity. The result actually would be an averaging process for the strengths of the four plates. Each of the eight flanges along the long edges of the tube would tend to act in unison at the inception of failure.

Mode Shapes

As might have been expected, various mode shapes were observed in the biaxially compressed tubes. When N_y was applied alone, the buckle consisted of one transverse half wave. It was similar to a classical wide column buckle. Most of the failures in the biaxially compressed tubes exhibited this buckle form.

The three lobe longitudinal loading buckle was not observed in any biaxially failed tube. However, it did occur at an intermediate loading phase in several of the tests. One of the most interesting aspects of the behavior of the biaxially loaded specimens of large b/t was the manner in which the buckles began as classical three lobe buckles at N_y less than failure and then snapped into the wide column form at failure.

From the standpoint of significance to the project, the tests on specimens 3-90-11 and 6-90-16 are the most important. They were planned to test whether the loading sequence would be important to the ultimate strength of a plate in combined loading. Since it involves pressure also, that result is deferred to that subsequent section of this report.

Wide Columns

The experimental buckling coefficients for wide columns appear in Table 8, while the buckle shapes appear in Fig. 31.

Table 5. Strength Data

b/t	Model No.	P_x lb.	P_y lb.	p [a] psi	Load Sequence	σ_x [b] ksi	σ_y [c] ksi
30	1-30-7	4060	-	-	N_x	36.91	-
30	1-30-8	3810	-	10.6	p N_x	36.63	-
30	1-30-11	2420	2600	-	N_x N_y	23.30	22.80
30	1-30-12	800	3400	-	N_x N_y	7.70	29.80
30	1-30-14	1350	3600	-	N_x N_y	13.00	31.50
30	1-30-17	2800	3200	-	N_x N_y	26.90	28.00
30	1-30-16	-	3040	-	N_y	-	26.60
30	1-30-2	4000	1335	-	c	38.50	11.70
50	1-50-6	5500	-	-	N_x	30.47	-
50	1-50-7	5330	-	10.6	p N_x	30.46	-
50	9-50-15	5540	1510	-	N_y N_x	31.60	7.94
50	9-50-12	-	2100	-	N_y	-	11.02
50	9-50-11	4800	2000	-	N_y N_x	27.40	10.50
50	9-50-13	2960	2600	-	N_x N_y	16.88	13.65
50	9-50-17	3500	1800	-	N_y N_x	19.95	9.46
50	1-50-16	2960	3500	10.4	N_x p N_y	16.90	18.40
50	1-50-18	-	2660	9.9	p N_y	-	14.00
50	9-50-14	1380	2680	-	N_x N_y	7.88	14.10
50	1-50-19	3580	2240	30	N_x p N_y	20.40	11.77
70	2-70-3	5060	-	-	N_x	20.32	-
70	7-70-5	5260	-	10.6	p N_x	21.30	-
70	7-70-1	5060	-	-	N_x	20.32	-
70	8-70-13	3800	2940	-	N_x N_y	15.39	11.04
70	8-70-15	2530	2610	-	N_x N_y	10.24	9.81
70	10-70-18	1270	2990	-	N_x N_y	5.14	11.22
70	2-70-6	-	1470	-	N_y	-	5.53
70	2-70-16	3800	2440	10.9	N_x p N_y	15.39	9.18
70	7-70-12	2530	2440	10.3	N_x p N_y	10.24	9.18
70	2-70-19	1270	2480	10.5	N_x p N_y	5.14	9.32
70	10-70-17	0000	1500	10.0	p N_y	0	5.64
70	7-70-14	2530	2300	16.	N_x p N_y	10.24	8.64

b/t	Model No.	P_x lb.	P_y lb.	p [a] psi	Load Sequence	σ_x ksi
90	9-90-1	5250	-	-	N_x	16.43
90	10-90-3	5360	-	-	N_x	16.65
90	8-90-5	5090	-	10.6	p N_x	16.00
90	9-90-4	5130	-	10.5	p N_x	16.11
90	3-90-8	2650	3860	-	N_x N_y	8.34
90	3-90-11	2650	2290	11.6	N_x p N_y	8.34
90	10-90-7	3980	3690	-	N_x N_y	12.50
90	3-90-18	3980	2000	10.8	N_x p N_y	12.50
90	8-90-10	1330	3480	-	N_x N_y	4.18
90	8-90-9	1330	2535	10.6	N_x p N_y	4.18
90	8-90-6	0000	1520	10.5	p N_y	0
90	3-90-19	0000	1325	-	N_y	0
90	8-90-12	2650 530	2230 3200	-	e	8.34 1.67
90	6-90-16	2650	2340	10.6	N_x N_yp [f]	8.34

a Internal vacuum except for 1-50-19 (30 psi internal p
7-70-14 (16 psi internal pressure)

b $P_x/[4bt(1 - t/b)]$

c $0.707\ P_y/3bt$

d $\sigma_x \rightarrow 15.0$ ksi, $\sigma_y \rightarrow 11.7$ ksi, $\sigma_x \rightarrow 38.5$ ksi (Failure)

e $\sigma_x \rightarrow 8.341$ ksi, $\sigma_y \rightarrow 6.531$ ksi, $\sigma_x \rightarrow 1.67$ ksi, $\sigma_y \rightarrow$

f Failed 1 to 2 Minutes after Vacuum was Applied

Table 6. Experimental Buckling Data

b/t	Model No.	P_x lb	σ_x ksi
70	7-70-1	4240	16.82
90	9-90-1	2930	9.04

Table 7. Centerline Measured Residual Stresses

b/t	30	50	70
σ_r ksi	14.2	8.5	4.8

Table 8. Wide Column Failure Data

b/t	30	50	70	90
k_y	0.91	1.05	1.02	1.11

The average of these four values is 1.05 compared to the theoretical value of unity. It was obtained by transposing Eq. (6) to the form

$$k_y = 1.105\ (\sigma_{yu}/E)(b/t)^2 \tag{31}$$

The measured value of the applied stress, σ_{yu} was obtained from Table 5.

RESIDUAL STRESSES

Introduction

Data on the hypothetically excellent control of residual stresses by the electron beam welding process were found to be inapplicable to the specimens fabricated for this investigation. This section details the basis for the belief that the residuals should have been small, describes the experiments to measure the residuals, and compares the current results to those of previous investigators.

Numerous tests and extensive literature analysis were conducted by Rao and Tall at Lehigh (Ref. 9). However, the measurements were made by comparing the lengths of scribed lines 8 to 10 inches long, before and after welding, on plates in which waviness might have occurred after welding as a result of which some of the conclusions may have been vitiated. Dwight and Ractliffe[1] (Ref. 2) measured residuals by generating pseudo-welds along the free edges of several test plates. They measured residual by extensometers in the plate interior. The current study employed bonded electric strain gages together with a new method of trepanning which is felt to furnish data of high reliability because of the achievement of excellent agreement of buckling theory and experiment on the effect of residuals in the current project.

Previous Status

Analyses were conducted by Buehler (Ref. 10) to determine the difference between the residuals from TIG welding and electron beam welding. Data were obtained on 0.062 inch thick 4340 steel sheets. The influence was determined by conducting microhardness surveys in the weld region and beyond into the plate region well beyond the weld zone. The hardness readings were then converted into stresses through the use of a standard hardness-yield conversion chart for steel.

The results are shown graphically in Fig. 18 as stress in terms of the distance from the weld centerline expressed as a multiple of the plate thickness. Two features are of prime importance. The plate stress at the weld centerline exceeded the base metal yield strength by about 25 percent, and the width of the hardened zone was only about 2/3 of the plate thickness on either side of the weld centerline. The

1. More recent data (Dwight and Moxham, "The Structural Engineer", Feb. 1969) will be examined in a subsequent investigation.

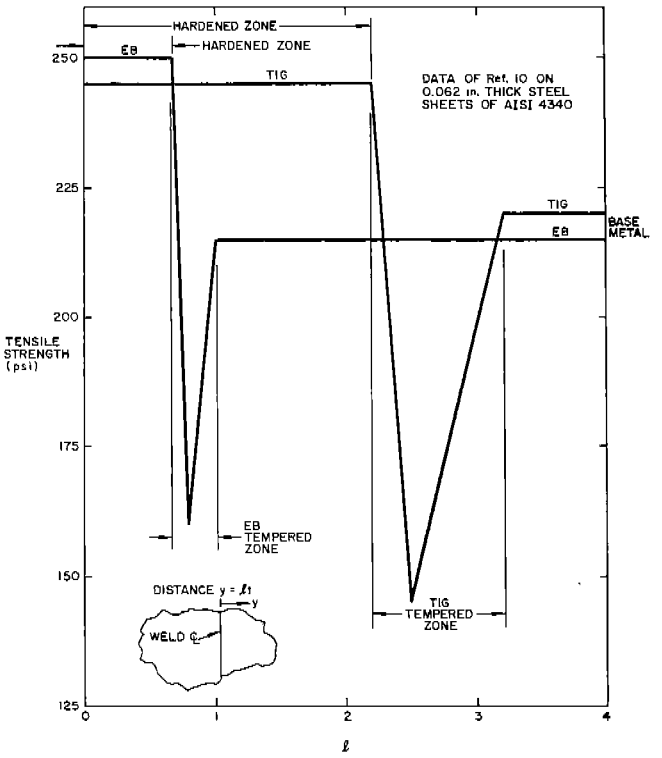

Fig. 18. Material Strength Variations in the Region of a Weld

resulting plate centerline compression stress would have been only about 5 percent of the yield for b/t = 30 and would have been almost negligibly small for the larger b/t plates of the current project.

Welding Procedure for Boxes

The plates for the square tube tests were sheared from the annealed stock sheets and then were milled to size. The final edge cuts were made in a milling machine at high rotation speed and low feed rate to minimize the induction of residual stresses. The cuts were no deeper than 0.010 inches.

As preparation of the plates for welding, they were clamped in proper orientation against an aluminum mandrel which was square in cross section. This provided accurate positioning of the plates together with heat sink action. The mandrel was rotatable in the vacuum chamber of the EBW apparatus so that all four corner welds could be accomplished in one pumpdown.

The welds were made at 26 kilovolts and 10 milliamperes with the work held 5 inches from the gun at a feed speed of 100 inches/minute. The beam was approximately 0.010 inches wide at the work surface.

After completion of welding the boxes were surface ground on each end to the length and squareness tolerances which are reflected in the sketches of Fig. 8. A rigorous inspection was conducted by the fabricator after grinding. The boxes were inspected again for flatness

and general quality of the workmanship. All dimensions were measured to the nearest 0.0001 inch.

Prior to testing, the ends of each box were surface lapped to insure maximum uniformity of contact with the loading heads, which were flat and square to within 0.0001 inches. The transversely loaded boxes required preparation of the long edges before testing. This consisted of a surface grinding at 45 degrees to the planes of the plates which comprised the boxes. The grinding was applied to a depth of 0.010 inches to achieve the desired contact uniformity.

General Character of Residuals

A conceptual sketch of the residual stress distribution in a welded plate appears in Fig. 19. This agrees with with the general nature of residuals measured by Dwight and Ractliffe and by the current investigators. The curves are shown smooth and symmetrical, which may be somewhat simplified as compared to actual stresses.

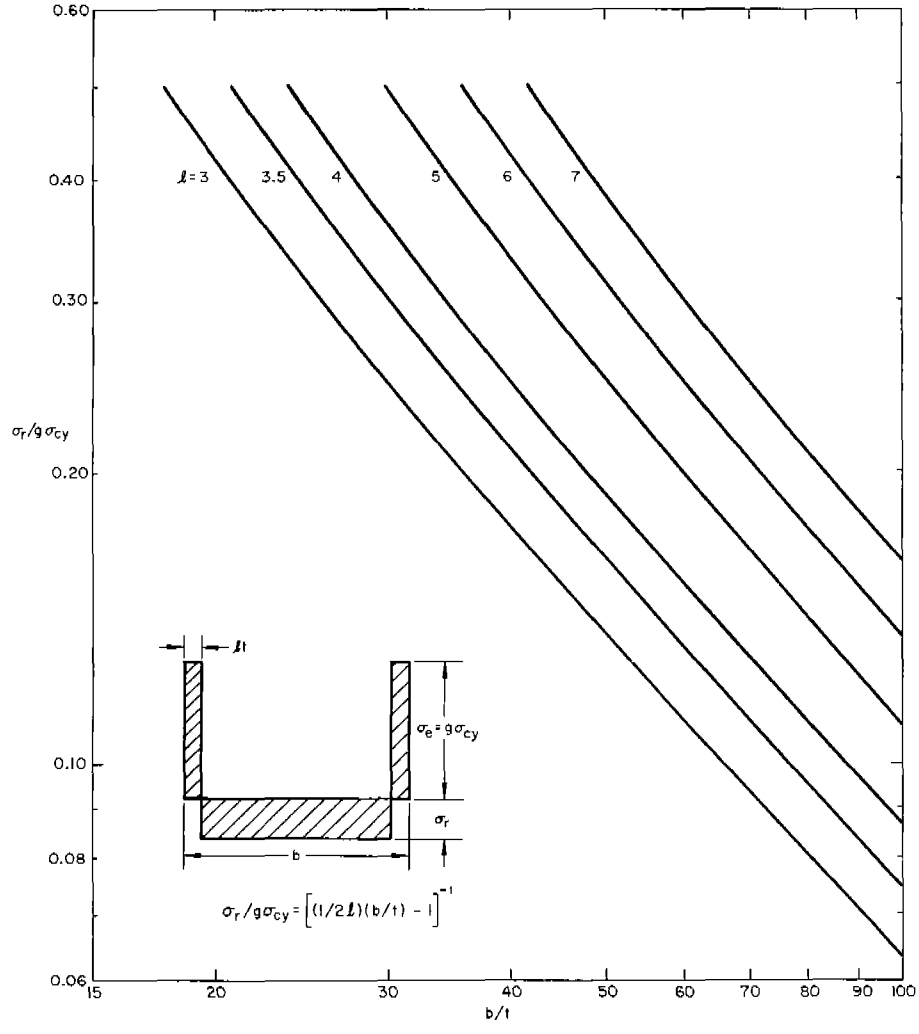

Fig. 19. Theoretical Residual Stress Curves

The sketches of Fig. 20 depict the model for residual stress induction. The behavior is self-evident from the sketch. If the idealized rectangular distribution is assumed to be a close approximation to the actual distribution, then a simple force balance yields

$$2\ell t\sigma_e = 2g\ell t\sigma_{cy} = (b - 2\ell t)\,\sigma_r \qquad (17)$$

which may be graphed as shown in Fig. 19.

Dwight and Ractliffe reported values of ℓ for stick-welded plates on the assumption that g = 1. However, measurements were made during this investigation which show that the edge stress can be much larger than σ_{cy}, which agrees with the results of Rao and Tall (Ref. 9), Buehler (Ref. 10) and others. Hence the use of the multiplier, g in Eq. 17. Furthermore, the manner of measurement used by different investigators raises questions as to the proper procedure, as discussed above.

Trepanning Procedure

In the current study, a single pair of longitudinal gages was used at the plate centerline after having found, from preliminary tests, that transverse gages at the centerline only registered the Poisson component of the basically uniaxial residual stress field. The trepanning procedure was used to reveal the weld centerline stresses and the distribution of stresses from the weld centerline to the plate centerline. It involved the machining of narrow strips from each edge of the plate. As each strip was removed, the longitudinal stress theoretically relaxed elastically across the entire plate in a uniform manner. The details of the stress increment relations appear in Fig. 21. When the entire weld region was removed, the plate should have been completely relaxed and the longitudinal strain accumulated in the center gages should equal the residual before trepanning, except for the reversal in algebraic sign.

The data from the shaving operations appear in Fig. 22. The reconstructed residual stresses are shown in Fig. 23, which reveals edge stresses considerably beyond yield, in agreement with Ref. 9, for example. Furthermore, the details of the stress fields agree with the general nature of those obtained by Rao and Tall, and by Buehler.

The tension region is much larger than in Fig. 18 which is based on hardness measurements. The edge stresses of the specimens in the current study were of the order of 45 to 50 ksi, as compared to the material yield of 39.2 ksi. Therefore, g was of the order of 1.25.

The wider edge band stress field found in the current studies accounts for the higher plate center residuals. Evidently, the narrow zone of increased hardness at the weld does not account properly for the stress distribution which was obtained by Buehler through use of the relation between hardness and yield strength.

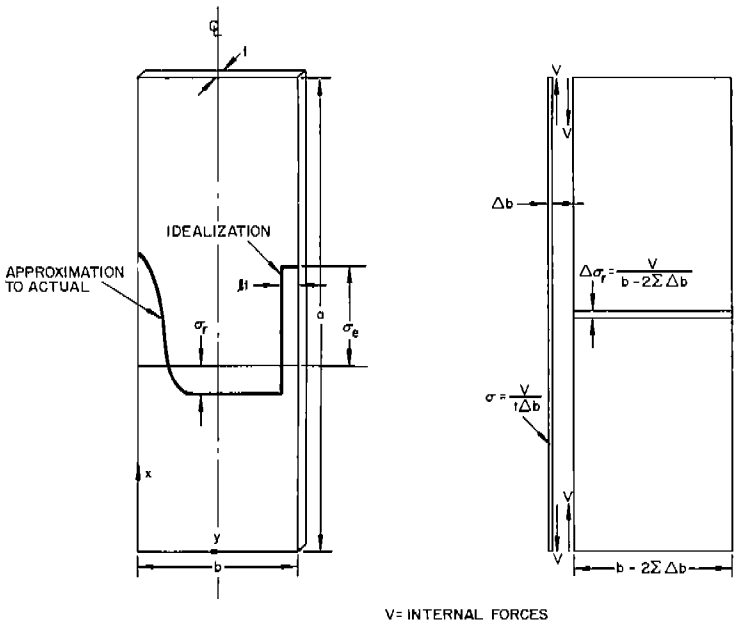

Fig. 20. Simplified Residual Stress Field Showing Balance of Internal Forces

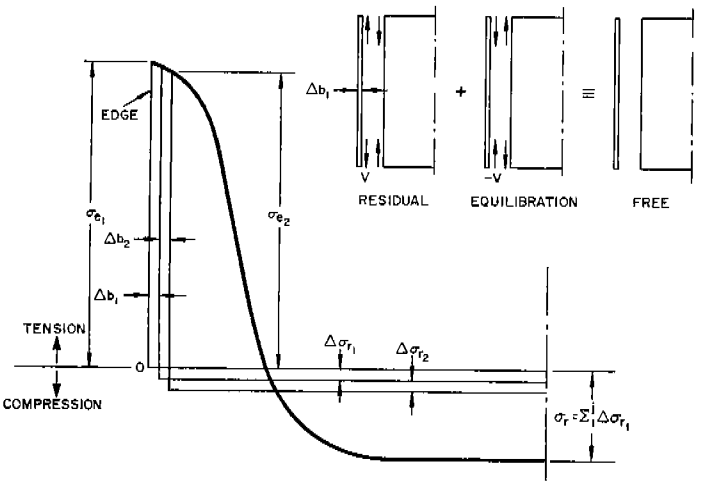

$$\sigma_{e_1} = \frac{b-2\Delta b_1}{2\Delta b_1}\,\Delta\sigma_{r_1}$$

$$\sigma_{e_2} = \frac{b-2(\Delta b_1+\Delta b_2)}{2\Delta b_2}\,\Delta\sigma_{r_2} - (\Delta\sigma_{r_1})$$

$$\sigma_{e_j} = \frac{b-2\Sigma_1^m \Delta b_i}{2\Delta b_m}\,\Delta\sigma_{r_m} - \Sigma_1^{m-1}\Delta\sigma_{r_1}$$

Fig. 21. Details of Edge Showing Procedure to Reveal Residual Stress Field

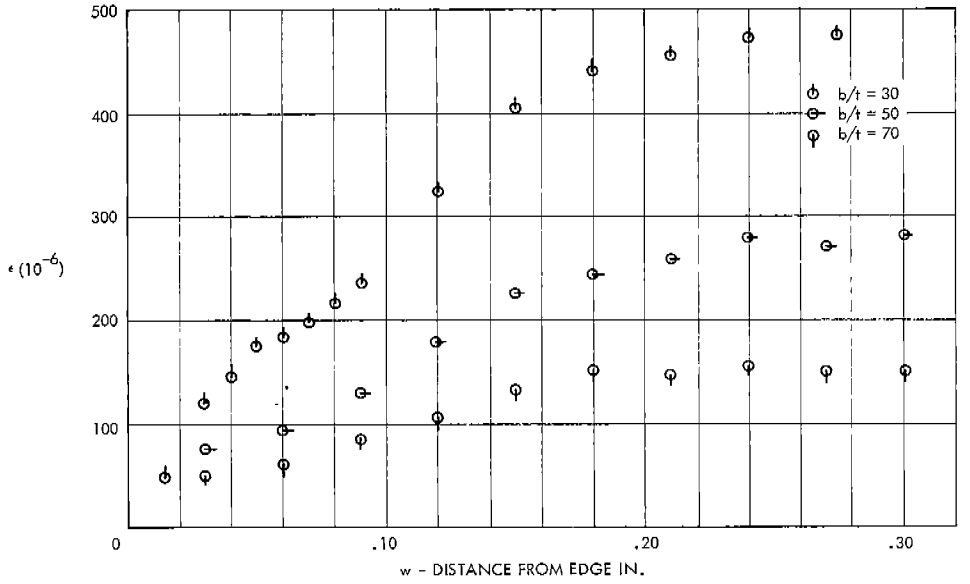

Fig. 22. Strain Gage Data from Shaving Operations

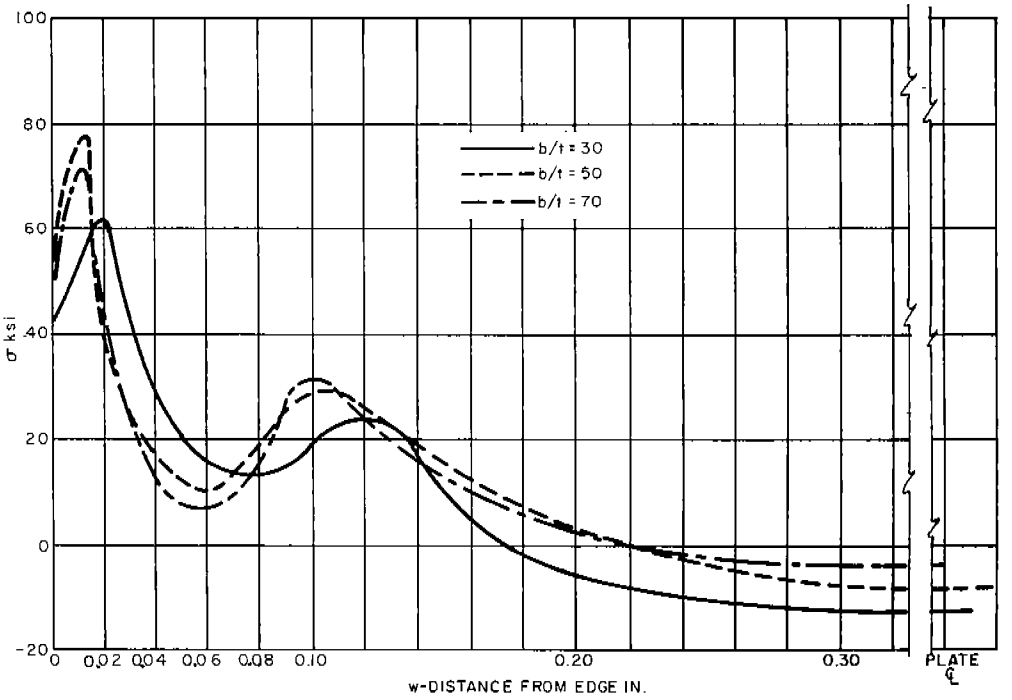

Fig. 23. Residual Stress Distribution

Residual stress curves are drawn through the current test data and the test data of Dwight and Ractliffe in Fig. 24. The curves were constructed from Eq. (17). The fit to the current experimental data was made with $g = 1.25$ and $\ell = 3.5$. In the absence of a reported value for g in Dwight and Ractliffe's results, this was assumed to be unity, although it may be contrary to the evidence in the literature, while ℓ was chosen at an average value of 7 for this data.

By performing the operations described above, the σ_r/σ_{cy} curve was converted to the $a\sigma_r/\sigma_{cy}$ curve for the two sets of data. These were then subtracted from the bottom of the scatter band of the older strength data, as shown in Fig. 24, since the current annealed plate strength data, and the data of Ref. 2, appear to lie generally along that line. A point-by-point comparison did not appear appropriate at the present time because of the meager data and the absence of specific residual stress information for each specimen.

As can be seen, the influence of residuals diminishes with decreasing b/t. For b/t greater than 60 the residual apparently may be subtracted from the annealed or residual-free curve without diminution. The transition zone between these extremes (from fully effective residual to a vanishing fraction of the residual) appears to occur in the b/t range from 45 to 60. Below $b/t = 45$ (and certainly at $b/t = 30$) the large residual stresses appear to impose no penalty on strength. The test of this prediction is the confrontation with the experimental data which occurs in the following section.

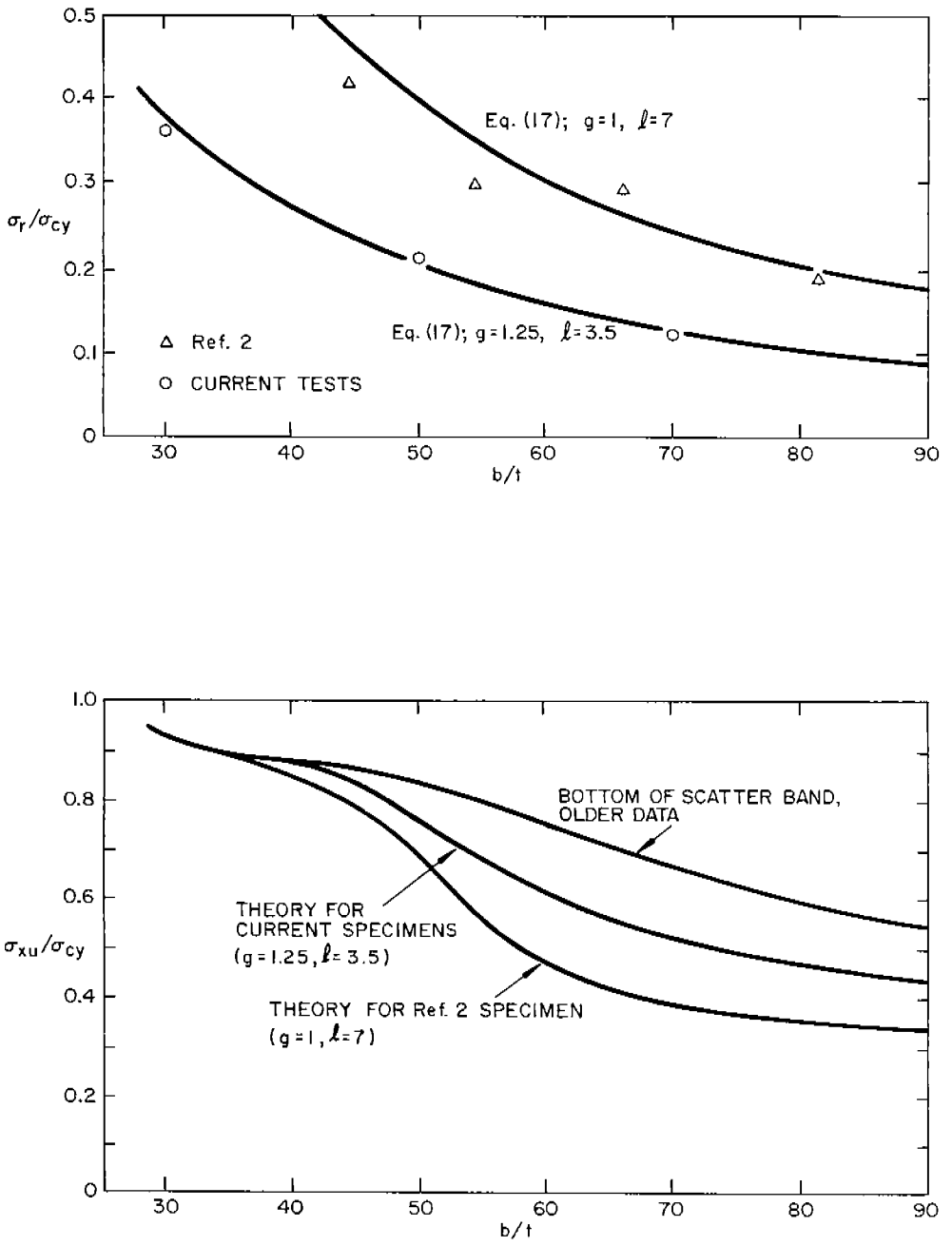

Fig. 24. Theoretical Effect on Compressive Strength of Residual Stresses in Plates

DISCUSSION OF UNIAXIAL COMPRESSION DATA

Historical Review

For several decades the basic source of data for determination of the uniaxial longitudinal strength of ship plates has been the curve derived from the experimental results obtained at the Experimental Model Basin (more recently the David Taylor Model Basin, and currently the Naval Ship Research and Development Center) by Frankland (Ref. 11), Vasta (Ref. 12) et al. The scatter band for the data appears in Fig. 25 along with the plot of the equation derived from the data,

$$\sigma_{xu}/\sigma_{cy} = 2.25F - 1.25F^2 \tag{18}$$

where

$$F = (t/b)(E/\sigma_{cy})^{1/2}$$

The experiments were conducted on a variety of steels, and on one aluminum alloy. Care was taken in the design of the experiments and in the conduct of the tests to achieve simple support along all four edges of the plates, each of which was loaded individually. The models were small relative to ship dimensions. Thicknesses were of the same order as the models in the current investigation (that is, 0.030 inch).

More recently, the needs of the aircraft industry stimulated tests on aluminum models. Among the best known data are the results reported by Needham (Ref. 13) who subjected square and rectangular tubes to compression forces and related the ultimate strengths to that of a long, hinged flange. He fitted the data to the relation

$$(\sigma_{xu}/\sigma_{cy})(\sigma_{cy}/E)^{1/2} = (t/b)^{3/4} \tag{19}$$

Further investigations were conducted by the Model Basin Staff (Refs. 14, 15 and 16) on aluminums and steels, as were researches by Dwight and Ractliffe in England, for example. (An extensive general bibliography for this field of endeavor appears in Ref. 17.) These more recent data appear in Fig. 25 together with the outlines of the early Model Basin Data. They are also reproduced on the logarithmic plot of Fig. 26 to depict the character of the scatter band which results in order to assess the utility of the relation advanced by Needham (Eq. 19) who derived his result from such plots.

The information shown in Figs. 25 and 26, together with Eqs. (18) and (19), represent the status of uniaxial strength data at the inception of this project. From Fig. 25, which reveals the smaller amount of scatter for each group of data, a significant discrepancy is seen to exist between the earlier and the more recent studies. Recommendations have been made to employ relations other than Eq. (18) in

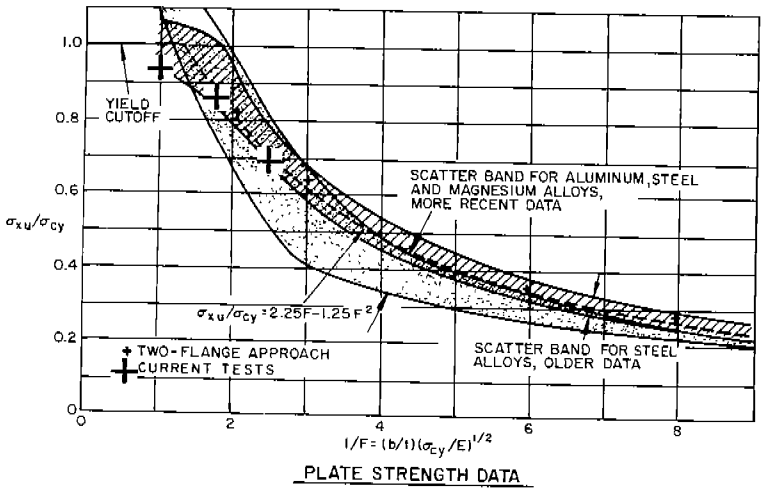

(Note: This is Figure 2 plus test points of current investigation.)

Fig. 25. Scatter Bands for Older and More Recent Strength Data

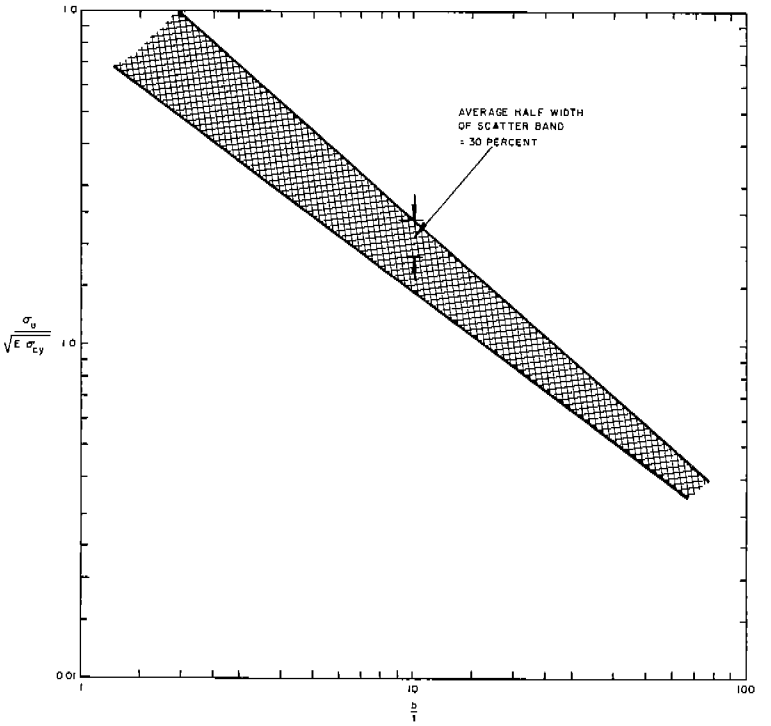

Fig. 26. Logarithmic Presentation of Strength Data Based on Eq. (19)

order to reflect this behavior (Refs. 2, 14 and 15, for example). Part of the current project was devoted to examination of these results in order to ascertain a possible explanation of the differences.

Strength Data from Current Investigation

The results in Figs. 25 and 26 ostensibly represent strengths of plates which were flat and free of residual stresses. Three test points were contributed to those results by this investigation. They appear as crosses which are seen to lie along the lower boundary of the scatter band of the earlier data. Buckle patterns appear in Fig. 27. The results agree well with those obtained by Dwight and Ractliffe (Ref. 2). Unfortunately, both sets of results lie in a range in which there is little to choose between the early and more recent data. However, one possible avenue may be open for seeking a resolution to the discrepancy between the early and more recent data. That would be through examination of the actual nature of the boundary conditions achieved during the tests.

Boundary Condition Evaluation

Boundary conditions usually relate to the control over the edge displacements normal to the plane of a plate, and to the rotational restraints imposed along the edges. During most test programs the restraint of deformations in the plane of the plate parallel to the edges is assumed to be nonexistent or is not considered. However, it is difficult to achieve ideal simple support in a practical test on a single plate. It probably is true that $w = 0$ in most plate tests. On the other hand, the difficulty of achieving complete rotational freedom in single plates is well known to experimentalists. It is also possible to effect some amount of longitudinal load transfer into the plate supports which run parallel to the edges. In fact, in spite of the considerable precautions which Dwight and Ractliffe employed to avoid this effect, they were able to measure 2 percent load transfer into edge restraints which actually were segmented and therefore might not have been deemed capable of transmitting longitudinal load.

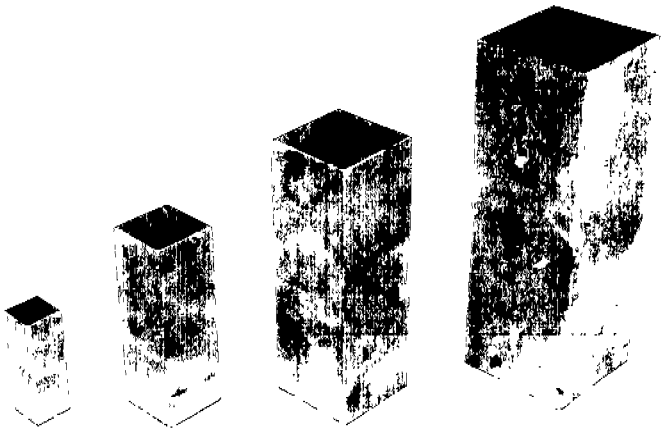

Fig. 27. Typical Buckles for Longitudinally Compressed Tubes

The unloaded edges of the early Model Basin tests were supported by slit cylinders bolted together finger tight. In a plate which is beginning to buckle, the tendency to form a longitudinal wave introduces transverse shear forces which distribute sinusoidally along each unloaded edge. If these forces are able to bind the plate within the edge restraints, then a small but measurable in-plane membrane restraint may result. If this had amounted to 5 percent of the axial force (against the 2 percent measured by Dwight and Ractliffe), the early test data would agree better with the more recent results. Since it is impossible to check that factor at this date, it cannot be made a basis for downgrading the early data.

Influence of Residual Stresses

Residual stresses have been measured by many investigators, as reported above. It has also been hypothesized (Refs. 1, 2) that the longitudinal compressive strength in the presence of residual stress may be related to the strength of a perfect plate (no residuals, absolutely flat) through the relation of Eq. (13) with $\alpha = 1$,

$$\sigma_r/\sigma_{cy} + \sigma_x/\sigma_{cy} = \sigma_{xu}/\sigma_{cy} \qquad (20)$$

The current data have shown that general use of Eq. (20) may lead to unnecessarily severe penalties for plates with small b/t.

Fig. 28 contains the prediction of the effect of residuals on longitudinal strength as reproduced from Fig. 24. The current strength data, and Dwight and Ractliffe's results, also are shown. In general, the agreement is good, and the trend of decreased influence of residuals on strength is clear. For b/t less than 55, only a negligible fraction of the measured residual was effective in reducing the strength of a perfect plate, whereas for b/t above 55 there was a rapid rise in the percentage of the residual which must be considered in determining plate strength. The data appear to indicate that Eq. (20) may be used only when b/t exceeds 70 on low carbon steel plates.

The trend in newer designs is toward small b/t, where the influence of residuals is small. In fact, the results at b/t = 30 reveal virtually no influence of residuals. (The slightly greater strength with residuals as shown in Fig. 28 must be charged to scatter.)

An additional test was conducted that yielded a result of considerable importance to the understanding of the critical strain approach to the role of residual stresses in plate strength determination. An unannealed specimen with b/t = 30 was axially loaded to 30 ksi. Deep Luders bands were observed across the full widths of the plates at several locations. The total hypothetical stress of about 45 ksi (residual plus load) would account for the presence of the Luders bands at this relatively low level of machine-applied stress.

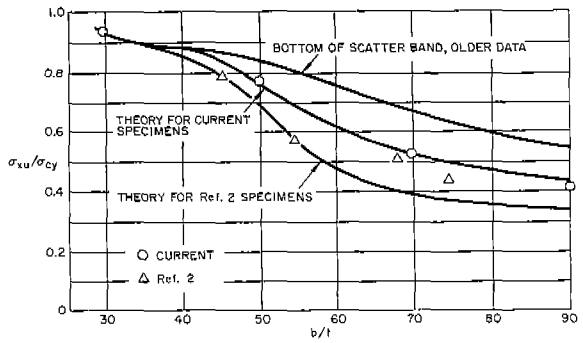

rig. 28. Effect of Residual Stress. Comparison of Theory with Experimental Data

In spite of the early appearance of the bands, they did not propagate. The load was maintained constant for 3 hours during which time no motion of the bands was discernible. A slight ridge line was detected at one of the bands, possibly indicative of a short buckle. The 1/32 inch buckle wavelength can be explained by the low tangent modulus of the stress-strain curve for the plate material at the knee of the curve.

At the end of the 3 hour constant-load period, the load was slowly increased until failure occurred, which was at 36.4 ksi, typical of the rest of the data for b/t = 30.

The results of this specimen support the critical strain approach to plate strength. No creep occurred during the 3 hour period since the end shortening supplied by machine head motion was not large enough to induce creep. If the machine load had reached the yield level, creep could have occurred in the specimen since the 3-column machine controls a force and not a deformation. As the machine load was increased, the residual compressive stress in the plates was transferred to the testing machine. The machine load did not directly increase the specimen stress. This may be seen qualitatively in Fig. 29 which depicts the plate at an edge strip. The edge strip is shown shorter than the center section before the two are assumed joined to generate the residual field. When the testing machine pressed down on the upper edge of the combination it diminished the edge tension and took up a portion of the center compression.

As the head continued to move down the edge strips returned toward the unstressed state and the total unloaded strain at the center ($\epsilon_e + \epsilon_c$), was transferred to the machine. The precise nature of the process requires measurements which could be made in a subsequent project. However, it is clear that the specimen strain corresponding to the machine load will exceed the end-shortening strain induced by the machine.

Buckling Stress Determination

Two experiments reveal the utility of the addition rule for residuals as applied to elastic buckling. In the first, a pair of strain gages was applied back-to-back oriented longitudinally at the center of one face of a specimen with b/t = 70. The difference in strain between the

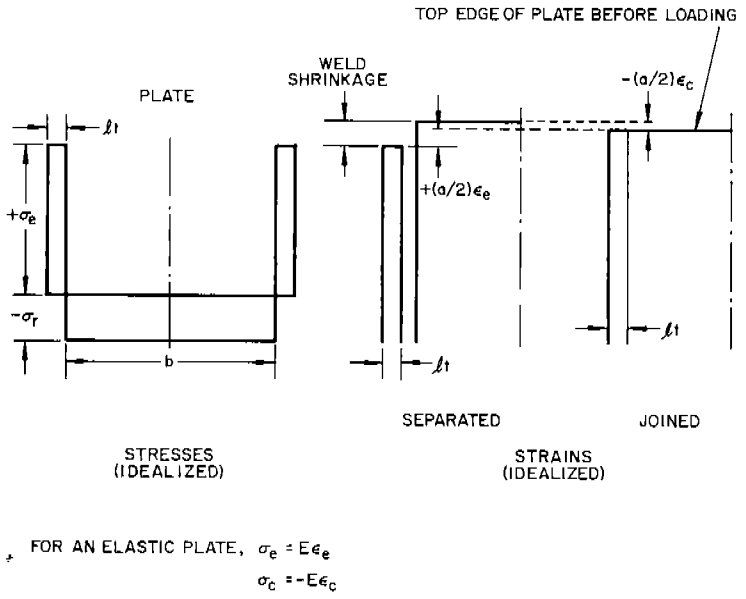

Fig. 29. Schematic of Testing Machine Interaction with Small b/t Specimens Containing Residual Stresses

two faces was recorded as a function of applied longitudinal compressive force and is shown in Fig. 30. This result is representative of the behavior of a plate with a small initial imperfection (Ref. 1). The solid curve on the figure indicates the difference between the theoretically perfect plate and the imperfect plate.

It is usually assumed that the curved portion of the load-lateral deflection relationship for the plate beyond buckling is parabolic in character. This provides a possible means for extrapolating the data from the upper segment of the curve to obtain a point of zero slope which can be identified as the load at which buckling occurred. This backward extrapolation for the plate of Fig. 30 yielded a critical stress of 16.8 ksi. The theoretical value of the buckling stress was 21.4 ksi from Eq. (5). If the residual stress value of 5.4 ksi (Fig. 24) is assumed to pertain to this plate, then the buckling stress obtained from the back extrapolation, together with the residual stress would yield a sum in reasonably good agreement with the theoretical buckling stress, which appears to substantiate the addition rule for elastic buckling in this b/t.

On a specimen for $b/t = 90$, a summing pair of gages yielded the curve of average strain as a function of applied load which appears on Fig. 30. The experimental buckling load must be taken at the beginning of the nonlinear zone in this case because of the insensitivity of this plot to the inception of instability. (In this case, the gages were used to reveal the postbuckling membrane strain pattern. Consequently, the application to the problem of residual stresses initially was a secondary consideration.) The data show experimental and theoretical critical values of 9.0 ksi and 13.0 ksi respectively, while the residual stress was 4.1 ksi (from Fig. 24). This also appears to support the addition rule.

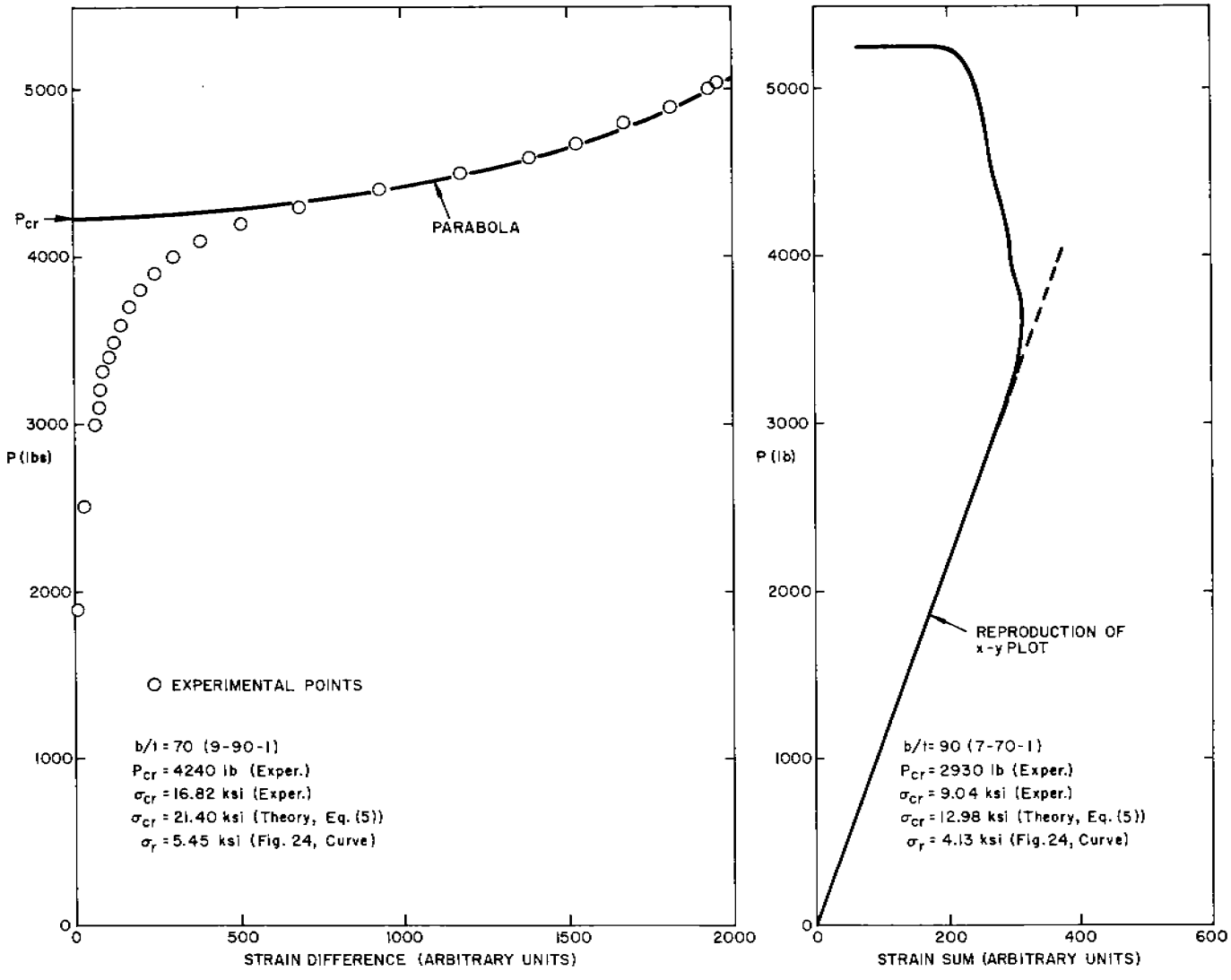

Fig. 30. Effect of Residuals on Longitudinal Compressive Buckling

DISCUSSION OF BIAXIAL COMPRESSION DATA

Introduction

The buckling and failure of rectangular plates under transverse compression, or under transverse compression in conjunction with longitudinal compression, was found to be radically different from the nature of uniaxial longitudinal compression. Apparently numerous factors may be involved in the complex manner in which buckling occurs and in which the buckling process influences the failure process. Furthermore, when transverse forces are present, the details of the methods of testing also seem to be much more critical than for uniaxial testing.

Some of these factors are summarized briefly, after which expositions are presented of wide column behavior and biaxial behavior.

Wide column buckle shapes are shown in Fig. 31.

Possible Influencing Factors

Numerous factors conceivably could affect the transverse and biaxial buckling and strength of rectangular plates. The shape and depth of initial imperfections, and the size of an imperfection relative to the size of a buckle, may be significant for transverse loads. The uniformity of material properties and the character of the residual stress field in the plate also could be relevant. Furthermore, the ratio of transverse loading to longitudinal loading would be a prime parameter, as well as the magnitude of load compared to critical stresses.

The departure from uniformity of load application during a test would control the possible localization of stresses throughout the plate and could lead to nonlinearity of stresses at various locations as the load is increased to failure. The shape of the stress-strain curve could be important since it would control the plasticity reduction factor, and actually it should be determined in biaxial compression for various ratios of transverse to longitudinal stresses for precise correlation of theory with experiment. Finally, the loading sequence might influence the postbuckling state of the plate thereby exercising control over the ultimate load level and failure mode shape.

The departures from unity and the increasing trend with b/t indicate possible uncertainties in the controllability of hinged boundary conditions at the loading head due to the presence of friction acting transverse to the long edges of the specimen. This might result in some rotational restraint along the loaded long edges as a result of the friction-induced unequal load between inner and outer plates. Some measure of this phenomenon may be obtained from evaluation of the data on the transverse strains.

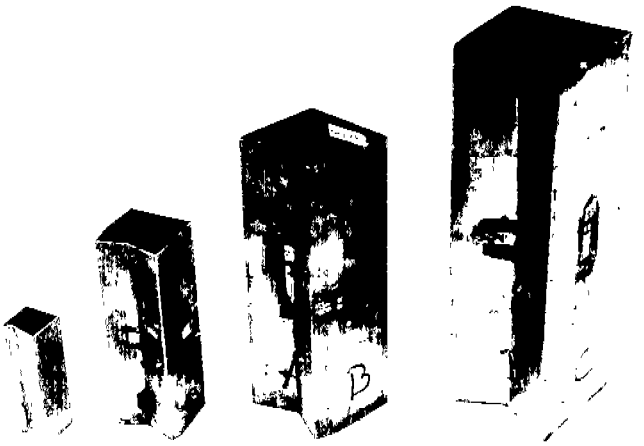

Fig. 31. Wide Column Buckle Photographs

The measurements of the transverse strains in the four wide columns appear in Fig. 32 which shows the theoretical value as well. The scatter between the greatest strain (at one end of the outer faces) and the smallest strain (at one of the inner faces) averaged about 20 percent except for b/t = 30 for which the difference was small. Therefore, an explanation for the trend of increased strength with b/t apparently must be sought elsewhere than in the effect of transverse friction. The influence of the longitudinal applied-strain/critical-strain ratio becomes a candidate for that explanation.

If the precepts of the critical strain approach are invoked to aid in the understanding of transverse and biaxial buckling and strength, then it follows that a prime candidate for a relevant parameter would be the ratio of the applied strain to the critical strain. The applied strain would include the strain arising from external forces and from internal residual stresses. The resultant strain ratio would indicate whether the plate is in the prebuckling or postbuckling configuration. This would indicate whether initial imperfections would be expected to be magnified significantly and whether transverse node lines were to be anticipated. In other words, the ratio should furnish a good indicator of the mode shape immediately preceding buckling and also preceding failure. Most importantly, since the residual and critical stresses involve b/t, then that parameter of the plate becomes one of the principal factors in identifying the plate behavior.

The following table reveals the residual stress as a function of the theoretical elastic longitudinal critical. It is apparent that the stress ratio (which is the same as the strain ratio) increases with b/t, which indicates the possible increase in susceptibility of the plates to initial formation of shallow longitudinal buckles before the transverse membrane stress was applied. Conceivably, the increasing trend may also reflect the biaxiality influence on transverse buckling as discussed in the Theory section. Intuitively, this latter action might be expected to diminish the transverse buckling stress. A precise answer awaits a complete analysis of this problem in a later project.

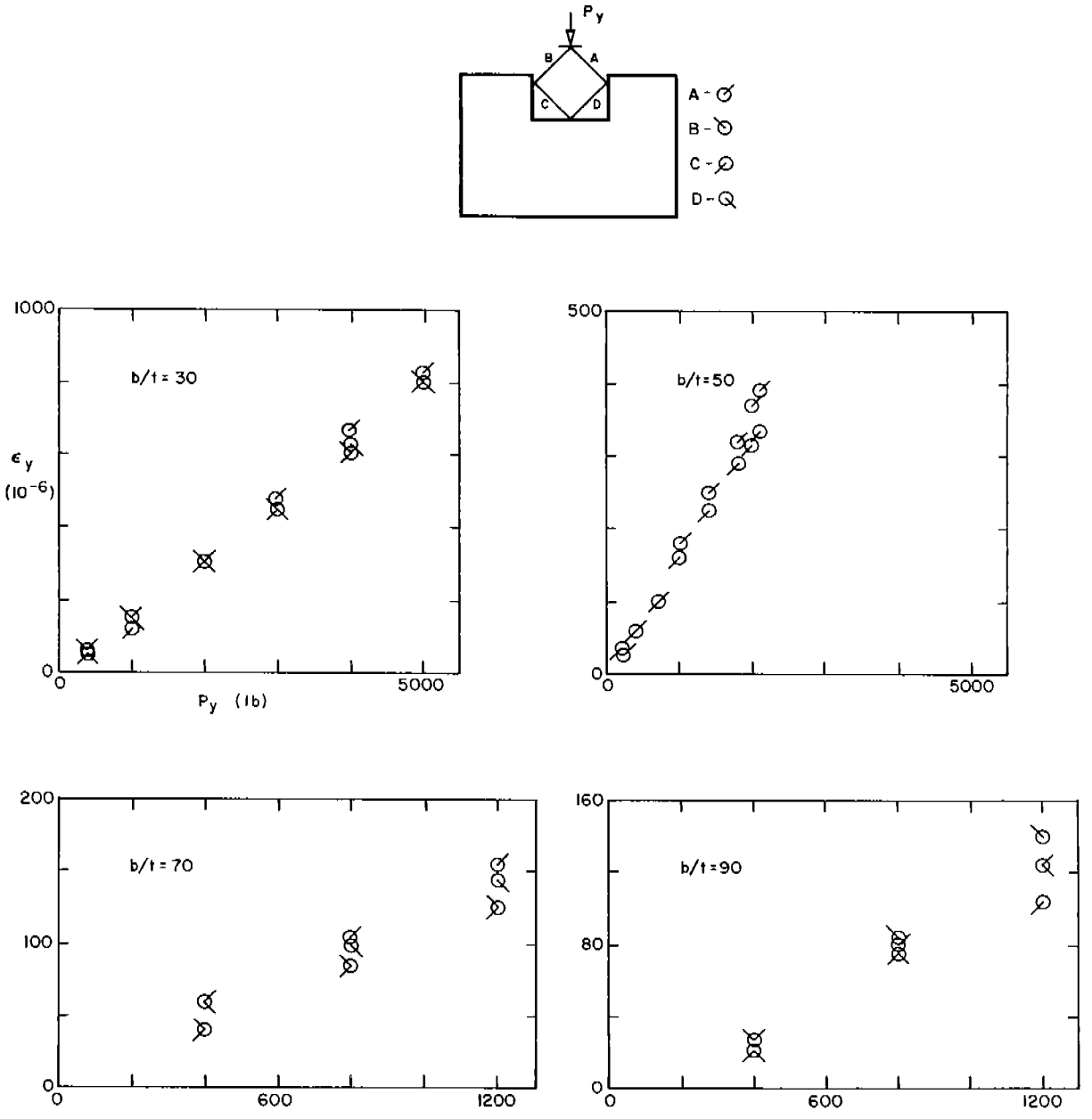

Fig. 32. Transverse Strains in Wide Columns

Table 9. Critical Strain Ratio For Wide Columns

b/t	30	50	70	90
σ_r (ksi)*	14.9	8.00	5.46	4.16
$\sigma_{x\,cr}$ (ksi)**	117.0	42.0	21.5	13.0
$\epsilon_r/\epsilon_{x\,cr}$	0.13	0.19	0.25	0.32

* Curve of Fig. 24
**Eq. (5)

For b/t = 30 a slight difference may be seen between the transverse strains in the two outer plates. This may have been the result of slightly nonuniform initial bearing of the unloaded edges, to a small amount of initial bowing of the box as a whole, and possibly to slight rotational slippage due to a diminution in alignment of the box within the transverse loading fixture.

Biaxial Compression

The experimental results for biaxial membrane stresses appear in Fig. 33. Typical buckles appear in Fig. 34. The data clearly show a large reduction in plate longitudinal strength when transverse membrane stress is applied in conjunction with longitudinal loading. The results are particularly pertinent in view of the trend toward small b/t in current shipbuilding practice. For b/t equal to 70 and 90 there appear to be large increases in transverse strength for longitudinally applied stresses which are as much as 75 percent of the uniaxial ultimate. It should be remembered that the results in Fig. 33 pertain to plates with residual stresses present.

Three regimes of behavior are involved in the plot of Fig. 33. For b/t = 30, for which the results appear to follow the trend of the hypothetical plate line of Fig. 3, failure may be assumed to have occurred as a result of biaxial plastic plate buckling. At b/t = 50 there appears to be a transition from plastic plate behavior to the multiple flange action which is typical of longitudinal compression strength. This latter behavior is offered as an explanation of the results for b/t = 70 and 90.

Table 2 summarizes the loads which theoretically could be supported by a pair of flanges for each plate type, based upon Eq. (10) and the assumption of a uniform distribution of the yield strength across the effective width of the flange. If more than 2 flanges are active, (h flanges, for example) in accordance with the hypothesis advanced in the Theory section, then the 2-flange force, P_2, can be multiplied by h/2. In this initial examination of the biaxial data 3 flanges were assumed

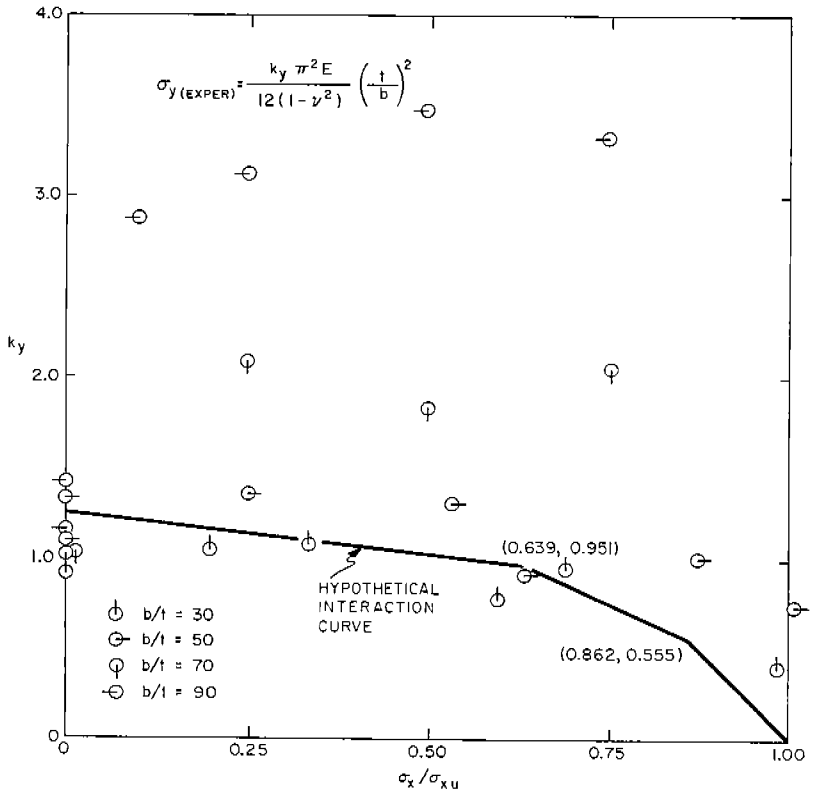

Fig. 33. Biaxial Strength Data

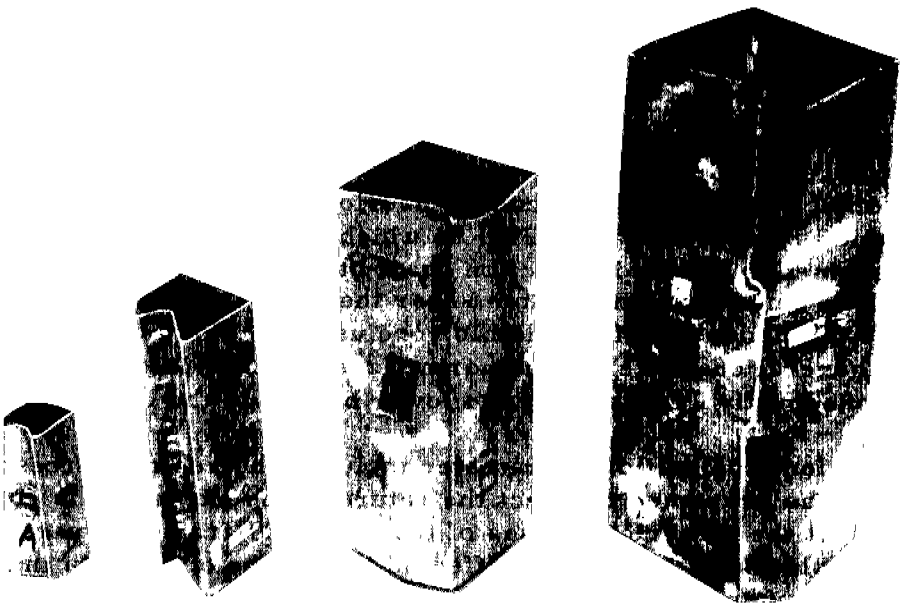

Fig. 34. Biaxial Buckle Photographs

active for b/t = 70 and 4 were assumed for b/t = 90. Actually, a different assumption would be appropriate for each N_x/N_{xy} since the buckle pattern which the longitudinal loading would induce exercises some measure of control over the number of interior ridge lines on the plate. However, the uncertainties in the boundary conditions make it impossible to define reliably the precise nature of the behavior for b/t greater than 30 in the current project. It is necessary to employ the evidence of the buckle pattern in each failed plate to provide support for the assumptions of the number of effective flanges in the plates.

The experimental justification for the choice of boundary conditions is available in the shapes of the ends of several test tubes. The buckle forms for typical wide columns may be seen in Fig. 34, while the results of several biaxial tests appear in Fig. 33. The similarity is evident where the ends of the biaxial test tubes were merely reacted by the longitudinal loading head plates. For the ends which were cemented to the plates and were internally restrained by cerromatrix plates, the edge behavior more closely approached the simple support shape typical of the longitudinally failed specimens shown in Fig. 27. However, the attainment of that condition is not certain.

If the capability of the longitudinal heads to enforce simple support depends upon the friction under the head, then the capability should be greater with smaller b/t for which the longitudinal pressure would be larger. Thus it is expected that two flanges could be effective at that location for b/t = 30 and 50, perhaps a flange would be partially effective for b/t = 70, and no effective edge flanges might be anticipated for b/t = 90. Typical transverse components of the biaxial fields appear in Fig. 35.

On the basis of the preceding assumptions concerning the number of effective flanges in the various plates, the biaxial data have been plotted in terms of the ratio of measured transverse strength to the theoretical multiple flange strength. The independent variable is the longitudinal strength ratio discussed previously and shown in Fig. 33. The plotted results appear in Fig. 36 which contains the normalized three-segment buckling interaction chart, the octahedral shear curve, and the two lines of the maximum shear theory. The size of the scatter band precludes drawing reliable conclusions. However, the trend has the general character of the normalized buckling interaction curve, which conservatively lies along the lower border of the band.

The longitudinal load parameter includes the residual stresses, which may be presumed to affect the nature of the curve. It is possible to substract the numerical values of the residuals from that parameter. It is probable that the residuals affected the nature of the data in Fig. 36. At this time no hypothesis can be offered to explain the character of the data.

The emphasis of the current investigation is upon the longitudinal strength of a rectangular plate, and the influence of various factors

upon that strength value. However, it was felt instructive, and germane to the scientific character of the investigation, to explore the effect upon transverse strength which is induced by the longitudinal loading.

It has been established in preceding discussions that the critical longitudinal strain field should play an important role in deciding the character of the transverse failure load and the associated behavior of the plate. The longitudinal strain is equal to the elastic strain resulting from all the longitudinal loads. This involves the externally applied force, P_x, and the internal forces resulting from the residual stresses of the current investigation. Therefore, the longitudinal strain ratio can be simplified to the form for elastic stresses

$$\epsilon_x/\epsilon_{x\,cr} = (\sigma_x + \sigma_r)/\sigma_{x\,cr} \tag{32}$$

since Young's modulus cancels.

The transverse strength parameter may be chosen the same as the ordinate of Fig. 33, or k_y. When it is plotted against the strain ratio as shown in Fig. 37, the points fall into a fairly well defined region for each b/t. The data clearly show how the longitudinal strain ratio affects the strength for each b/t. The transition between degradation and enhancement appears to be in the region of b/t = 50. The reference on the ordinate axis is the transverse buckling coefficient for a/b = 3.

The scatter in the data of each group may be attributed to the various factors enumerated at the beginning of this section. It is conceivable that control of the boundary conditions on the short edges may be most important. Furthermore, the loading sequence involved the application of N_x before N_y in every case except for the few identified in the figure. This might be important for large b/t in accordance with preceding discussions on the buckle pattern.

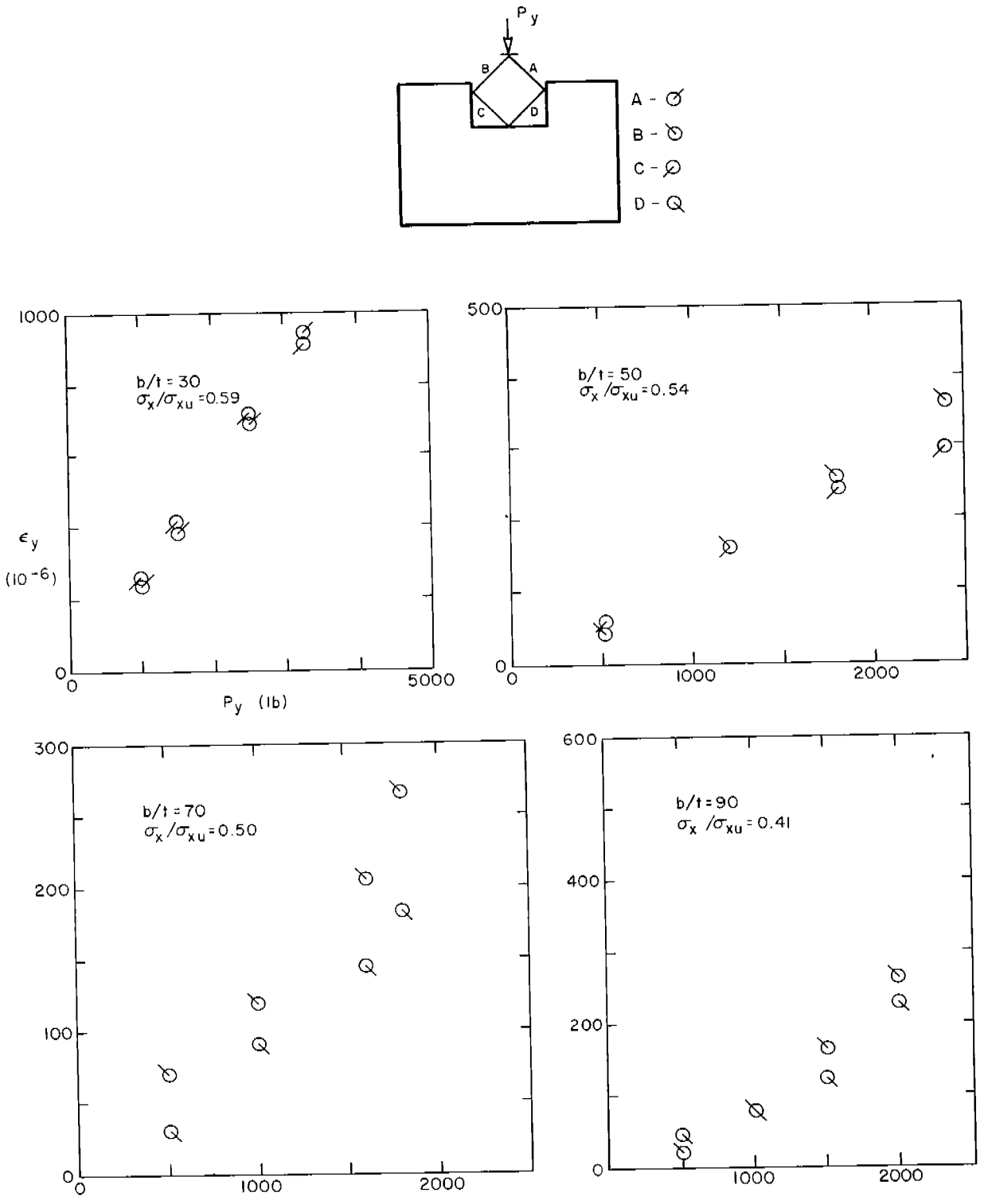

Fig. 35. Strains Due to Transverse Loads on Biaxially Compressed Plates

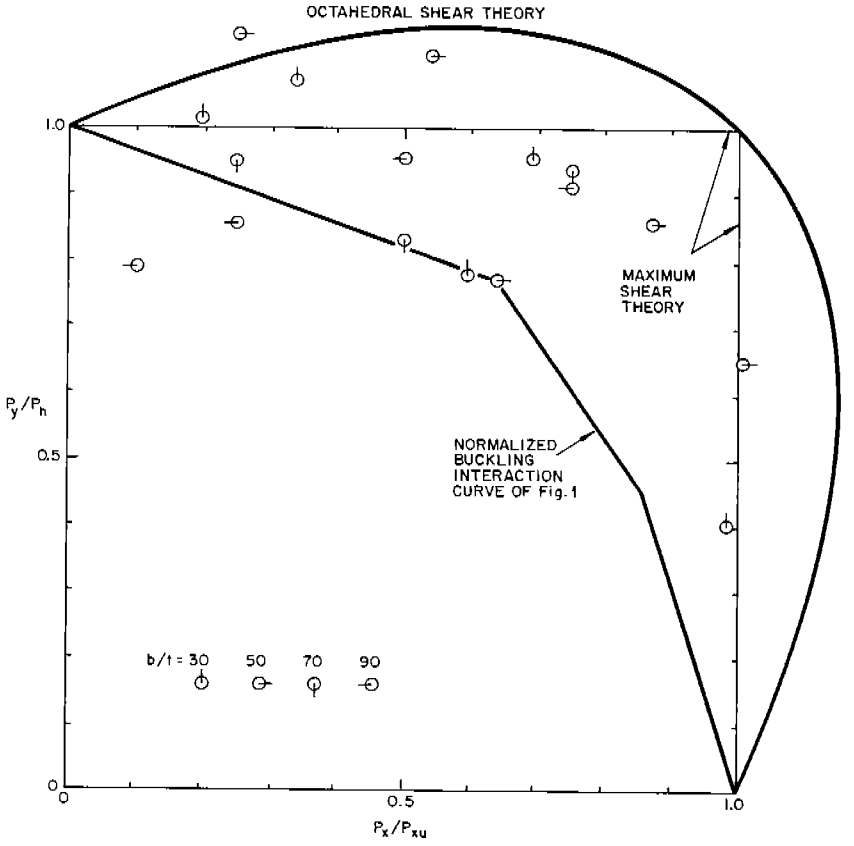

Fig. 36. Normalized Biaxial Strength Data

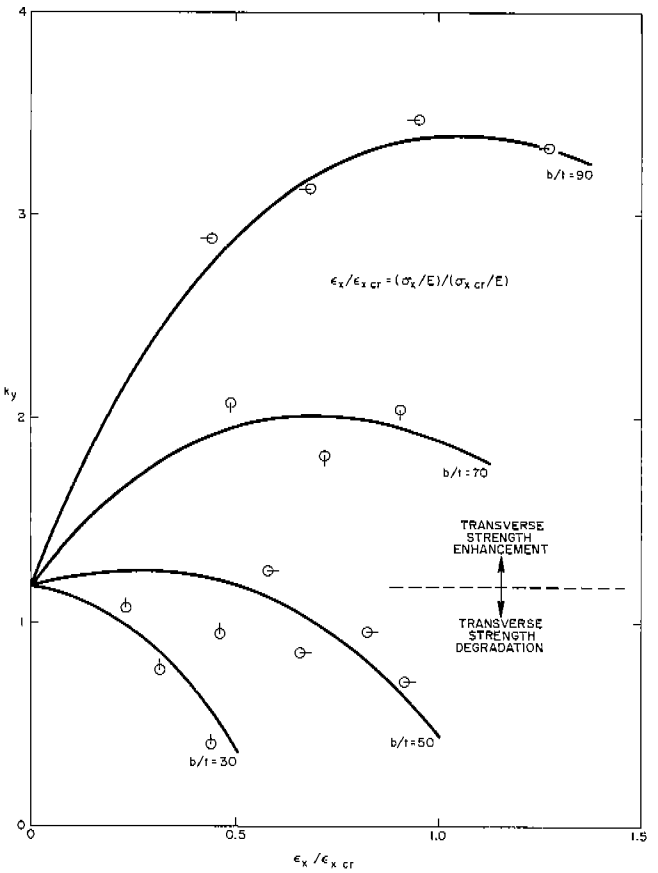

Fig. 37. Transverse Plate Strength as a Function of Longitudinal Strain Relative to Critical Strain

EFFECT OF NORMAL PRESSURE

Introduction

The current studies revealed little identifiable influence of normal pressure on longitudinal strength, or upon transverse strength with the lower b/t plates. However, for large b/t the effect appears to be significant. In fact, for b/t = 90 a large reduction of transverse strength was observed.

The theories which relate to the influence of normal pressure do not appear to be useful for predictive purposes. They relate to buckling (Ref. 7) and to the growth of transverse deflections rather than to strength, or to the algebraic addition of membrane and bending stresses (Ref. 3) which yields predictions that do not appear to relate to the experimental data.

In the absence of a theory or hypothesis with which to correlate the experimental data, the effect of pressure is presented in the light of an influencing factor. A predictive procedure is required before it is possible to discuss correlation of theory with experiment.

Effect of Pressure on Longitudinal Strength

In the presence of internal vacuum the failure mode shapes in the uniaxially compressed tube walls were basically the same as in the tubes under uniaxial compression alone. They displayed the three lobe classical form. The only observable difference was a slight increase in the buckle lengths in the centers of the plates with vacuum compared to the plates to which no normal pressure was applied. These may be seen in Fig. 38.

The data on longitudinal strength in the presence and absence of normal pressure appear in Table 10 which shows little change due to normal pressure. Both sets of data involve the presence of residual stresses. The table also contains the bending stresses induced at the plate longitudinal centerlines by the applied normal pressure. The bending stresses were calculated on the assumption of completely built in long edges because of the symmetry involved in the tubular construction.

As the table reveals, the bending stress was beyond yield for b/t = 90. For b/t = 70 it was about 60 percent of yield while for the lower b/t values it was much smaller.

Effect of Pressure on Biaxial Strength

The large pressure-induced reductions in biaxial strength are evident in Fig. 39 for b/t = 90, while moderate reductions were sustained for b/t = 70. The influence of pressure in the current investi-

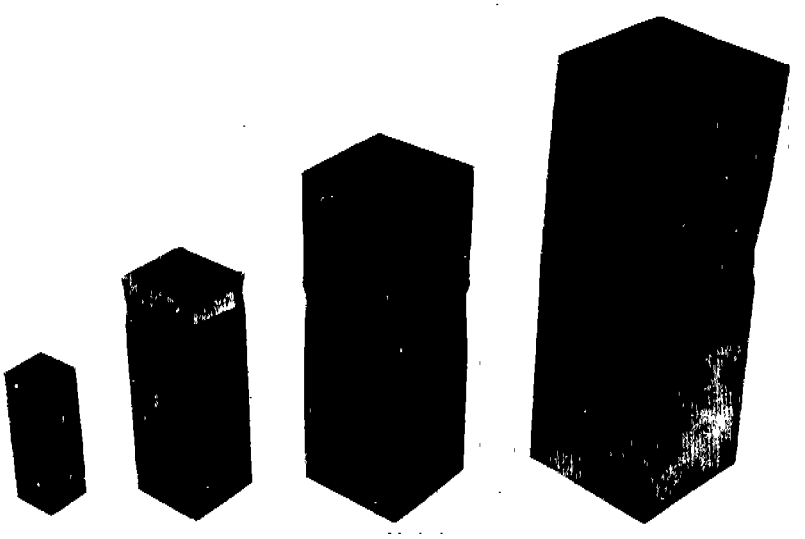

Fig. 38. Buckle Patterns for Longitudinally Compressed Tubes with Internal Vacuum

Table 10. Effect of Pressure on Longitudinal Strength

b/t	30	50	70	90
σ_{xu}, ksi[a] with pressure	36.63	30.47	21.30	16.00
σ_{xu}, ksi[a] no pressure	36.91	30.46	20.32	16.43
σ_b - ksi[b]	4.8	13.3	26.0	42.9

[a] Table 5 [b] $(p/2)\,(b/t)^2$ with p from Table 5

gations appears to have been negligible for b/t = 50, and consequently it was elected to bypass testing b/t = 30 in the current project. The 40 percent loss in strength for b/t = 90 may be explained on the basis of the bending stress induced by the normal pressure as shown in Table 10.

This strength loss apparently results from the combined stress type of phenomenon assumed by Timoshenko (Ref. 3). However, as was mentioned previously, an attempt to match Timoshenko's prediction with the data was not successful. Furthermore, an explanation is not readily available without extensive studies of other approaches.

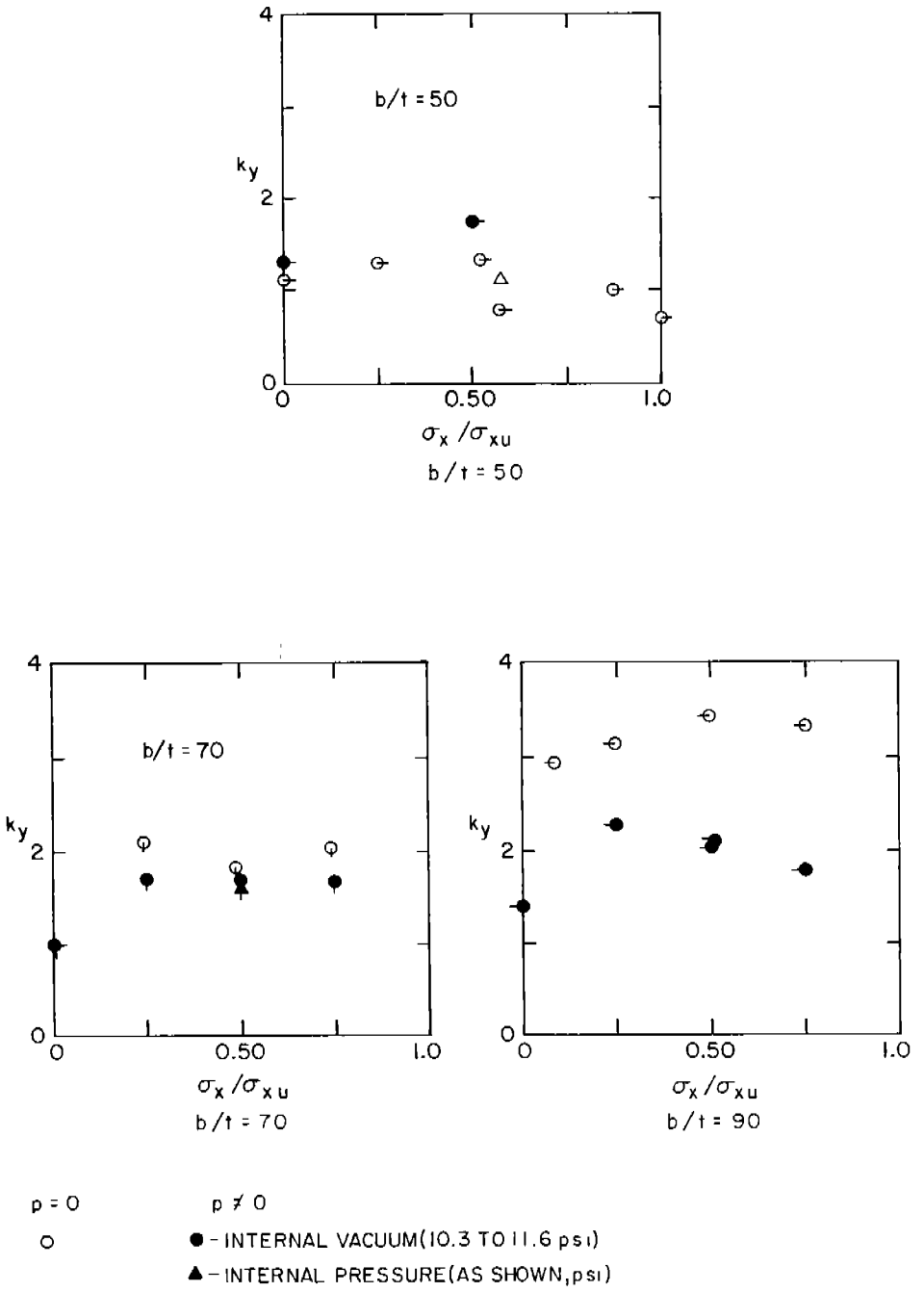

Fig. 39. Effect of Pressure on Biaxial Strength

The tests on specimens 3-90-11 and 6-90-16 were most important to the project since they identified the role of the pressure loading sequence as it affects plate strength in combination with biaxial membrane loading. The experiments were conducted on two tubes with $b/t = 90$. The two loading sequences are depicted in Fig. 40. In the first case, pressure was applied followed by N_x. Then N_y was applied to failure which occurred as a wide column. In the other case N_y was applied first, followed by N_x to the same value as previously. At that time a typical three lobe uniaxial type buckle was observed in the tube with the lateral deflection about the order-of-magnitude of the plate thickness. The pressure was then increased to the value of the previous test. Nothing happened at first. However, during the few seconds in which the testing machine controls were changed to apply more N_y, failure occurred before the load could be increased. At the time of failure the buckle pattern snapped (almost instantaneously) from the three lobe longitudinal form to the transverse wide column form.

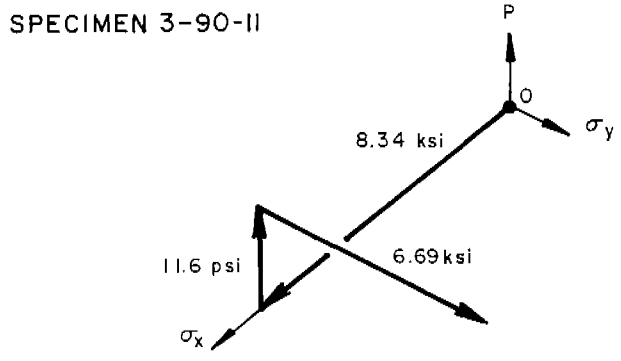

Fig. 40. Load Sequences for Tests 3-90-11 and 6-90-16

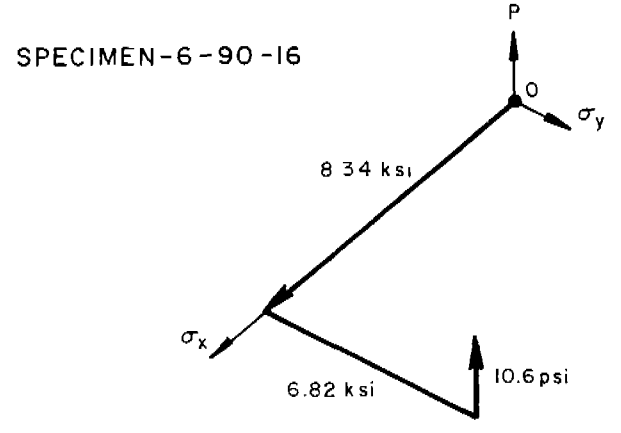

CONCLUSIONS

The following conclusions may be generally applicable. However, it must be borne in mind that the current tests were conducted on flat plates, fabricated from typically elastic-plastic steels, with $a/b = 3$, and with $t = 0.030$ in.

1. The failure of a plate under biaxial membrane loading is radically different from failure under longitudinal loading. For $b/t = 50$ or less a large reduction in longitudinal strength accompanies the application of transverse loading. For $b/t = 70$ and 90, there appears to be greater transverse strength in the presence of longitudinal loading. In these cases the failure mode appears to involve transverse flange strips, analogous to the two-flange hypothesis of longitudinal strength for plates with large b/t. For the smaller b/t plates the mode of failure appears to be that of plastic biaxial buckling.

2. It has been demonstrated theoretically and experimentally that the influence of welding residual stress on mild steel plate longitudinal strength under uniaxial compressive loading becomes insignificant at b/t less than 40. At b/t between 40 and 60 the percentage of the residual stress which influences strength is increased from 0 to 100. Beyond 60 the strength is reduced by the full amount of the residual stress. On the basis of the data displayed herein, it appears possible to predict the realizable longitudinal strength of a welded plate by direct utilization of the data on the welding process parameters induced by the welding.

3. Theory and experiment both indicate a significant influence of welding residual stress on the strength of a plate with $a/b = 3$ under uniaxial transverse membrane loading.

4. Current experiments appear to have demonstrated negligible influence of normal pressure upon uniaxial longitudinal compressive strength, which is in line with previously advanced hypotheses. The same may be said of biaxial strength for $b/t = 50$ or less. For greater b/t, however, a pressure of 10 psi was found to degrade the biaxial strength dramatically, with the degradation increasing rapidly with b/t and becoming as high as 40 percent at $b/t = 90$.

5. Small model tests were shown to agree with results from previously reported large scale tests.

6. It appears appropriate to consider a slight reduction in the design curve for longitudinal strength of unstiffened plates from that in current use in the United States. The reduction could amount to 10 percent in the present values of σ_{xu}/σ_{cy} for $(b/t)(\sigma_{cy}/E)^{1/2}$ greater than 2.5, with a gradual diminution in the reduction to zero at 1.5. This would bring the design curve into closer agreement with the latest data.

7. From the standpoint of minimization of scatter, the current method of relating strength appears to be the best of all those which have been advanced by various investigators. Although the current procedure displays σ_{xu}/σ_{cy} as a function of the parameter $(b/t)\,(\sigma_{cy}/E)^{1/2}$, which mixes material and geometric terms in the latter parameter, this possible objection would seem to be overridden by the fact that the width of the scatter band is less than in other plotting procedures in which the material properties are encompassed in one parameter that is plotted logarithmically as a function of the geometric parameter, b/t.

RECOMMENDATIONS

A vigorous program of experimentation and development of theory should be pursued to broaden the base of the data established during this investigation.

1. Studies should be conducted on plates with a/b between 1 and 3.

2. The influence of the shape of the stress-strain curve should be examined by experiments on materials with rounded knee type stress-strain curves.

3. The weld studies instituted in this investigation should be broadened to provide the design data necessary to implement the prediction procedure for the influence of residual stresses using the welding parameters and plate properties as the basic input.

4. Biaxial strength studies should be extended to acquire more data so as to permit resolution of the residual stress influences and boundary condition problems and to consolidate the hypotheses into theory. The influence of shear should be included also.

5. In order to demonstrate further the hypothesis that instability is not size-dependent, studies should be conducted on plates with thicknesses of the order of 0.060 in. The b/t range should be extended also.

6. Plates should be tested with controlled initial imperfections to provide the best possible correlation with strength predictions.

7. Stress analyses should be conducted of ships which have been lost at sea, or which have suffered severe damage from the action of the sea, in order to determine whether biaxial instability could account for the failure.

8. Syntheses should be performed to determine whether there may be size limitations on ships based upon the possibility of failure under biaxial loading.

Acknowledgements

The authors wish to express their appreciation to Mr. Angelo Colao for his assistance in designing the test equipment, and to Mr. Edward Suskevich for his contributions to the instrumentation of the specimens and the performance of the experiments. Mr. James Viall, the welding subcontractor, supervised the machining, welding and finishing of the models.

REFERENCES

1. Becker, H., "Feasibility Study of Model Tests on Ship Hull Girders", National Academy of Sciences, Ship Structure Committee Report SSC-194, May 1969.

2. Dwight, J. B., and A. T. Ractliffe, "The Strength of Thin Plates in Compression", Published in "Thin Walled Steel Structures", Ed. by Rockey and Hill, Gordon and Breach, N. Y. 1969, pp. 3-34.

3. Timoshenko, S., "Theory of Elastic Stability", McGraw-Hill, N. Y., 1936.

4. Bengston, H. W., "Ship Plating Under Compression and Hydrostatic Pressure" Trans. SNAME, 47, No. 80, 1939, pp. 80-116.

5. vonKarman, T., E. E. Sechler and L. H. Donnell, "The Strength of Thin Plates in Compression", Trans. ASME, APM-54-5, 54, No. 2, Jan. 1932.

6. Gerard, G., "Secant Modulus Method for Determining Plate Instability Above the Proportional Limit", Journal of the Aeronautical Sciences, 13, No. 1 Jan. 1946, pp. 38-45.

7. Levy, S., D. Goldenberg and G. Zibritosky, "Simply Supported Long Rectangular Plates Under Combined Axial Load and Normal Pressure", NACA TN 949, October 1944.

8. Hoffman, O., and G. Sachs, "Introduction to the Theory of Plasticity for Engineers", McGraw-Hill, N. Y. 1953.

9. Rao, N. R. N., and L. Tall, "Residual Stresses in Welded Plates", Welding Research Supplement, October 1961, pp. 468s-480s.

10. Anon., "A Technical Report on Electron Beam Welding". The Buehler Corporation, Indianapolis, Inc.

11. Frankland, J. A., "The Strength of Ship Plating Under Edge Compression", U. S. Experimental Model Basin Report 469, 1940.

12. Vasta, J., Unpublished U. S. Experimental Model Basin Progress Reports ca 1940.

13. Needham, R. A., "The Ultimate Strength of Aluminum-Alloy Formed Structural Shapes in Compression", Journal of the Aeronautical Sciences, 32, No. 4, April 1954, pp. 217-229.

14. Duffy, D. J., and R. B. Allnutt, "Buckling and Ultimate Strengths of Plating Loaded in Edge Compression", David Taylor Model Basin Report 1419, April 1960.

15. Conley, W. F., L. A. Becker and R. B. Allnutt, "Buckling and Ultimate Strength of Plating Loaded in Edge Compression, Progress Report 2 - Unstiffened Panels". David Taylor Model Basin Report 1682, May 1963.

16. Collier, J. S., "Ultimate Strength of Plating Loaded in Edge Compression - Effect of Adjacent Panels". Naval Ship Research and Development Center Report, April 1967.

17. Cooper, P. B., "Literature Survey on Longitudinally Stiffened Plates". Lehigh University Fritz Engineering Laboratories Report 304.2, September 1963.

UNCLASSIFIED
Security Classification

DOCUMENT CONTROL DATA - R&D

(Security classification of title, body of abstract and indexing annotation must be entered when the overall report is classified)

1. ORIGINATING ACTIVITY *(Corporate author)*
U. S. Naval Ordnance Laboratory
White Oak, Maryland

2a REPORT SECURITY CLASSIFICATION
Unclassified

2b GROUP

3 REPORT TITLE
Compressive Strength of Ship Hull Girder Part I Unstiffened Plates

4 DESCRIPTIVE NOTES *(Type of report and inclusive dates)*
October, 1970

5. AUTHOR(S) *(Last name, first name, initial)*
H. Becker, R. Goldman, and J. Pozerycki

6. REPORT DATE	7a. TOTAL NO. OF PAGES	7b. NO. OF REFS
October, 1970	61	17

8a. CONTRACT OR GRANT NO.
N00024-69-C-5413

b. PROJECT NO.

c.

d.

9a. ORIGINATOR'S REPORT NUMBER(S)

9b. OTHER REPORT NO(S) *(Any other numbers that may be assigned this report)*
SSC-217

10. AVAILABILITY/LIMITATION NOTICES
Unlimited.

11. SUPPLEMENTARY NOTES

12. SPONSORING MILITARY ACTIVITY
Naval Ship Systems Command

13. ABSTRACT

Three problem areas of Hull girder strength are biaxial strength(to account for the transverse membrane loadings induced by the sea), the influence of normal pressure loadings on strength, and the influence on strength of residual stresses induced by welding. Data on solutions to these problems were obtained during this project.

DD FORM 1 JAN 64 1473

UNCLASSIFIED
Security Classification

14. KEY WORDS	LINK A		LINK B		LINK C	
	ROLE	WT	ROLE	WT	ROLE	WT

INSTRUCTIONS

1. ORIGINATING ACTIVITY: Enter the name and address of the contractor, subcontractor, grantee, Department of Defense activity or other organization *(corporate author)* issuing the report.

2*a*. REPORT SECURITY CLASSIFICATION: Enter the overall security classification of the report. Indicate whether "Restricted Data" is included. Marking is to be in accordance with appropriate security regulations.

2*b*. GROUP: Automatic downgrading is specified in DoD Directive 5200.10 and Armed Forces Industrial Manual. Enter the group number. Also, when applicable, show that optional markings have been used for Group 3 and Group 4 as authorized.

3. REPORT TITLE: Enter the complete report title in all capital letters. Titles in all cases should be unclassified. If a meaningful title cannot be selected without classification, show title classification in all capitals in parenthesis immediately following the title.

4. DESCRIPTIVE NOTES: If appropriate, enter the type of report, e.g., interim, progress, summary, annual, or final. Give the inclusive dates when a specific reporting period is covered.

5. AUTHOR(S): Enter the name(s) of author(s) as shown on or in the report. Enter last name, first name, middle initial. If military, show rank and branch of service. The name of the principal author is an absolute minimum requirement.

6. REPORT DATE: Enter the date of the report as day, month, year; or month, year. If more than one date appears on the report, use date of publication.

7*a*. TOTAL NUMBER OF PAGES: The total page count should follow normal pagination procedures, i.e., enter the number of pages containing information.

7*b*. NUMBER OF REFERENCES: Enter the total number of references cited in the report.

8*a*. CONTRACT OR GRANT NUMBER: If appropriate, enter the applicable number of the contract or grant under which the report was written.

8*b*, &*c*, & 8*d*. PROJECT NUMBER: Enter the appropriate military department identification, such as project number, subproject number, system numbers, task number, etc.

9*a*. ORIGINATOR'S REPORT NUMBER(S): Enter the official report number by which the document will be identified and controlled by the originating activity. This number must be unique to this report.

9*b*. OTHER REPORT NUMBER(S): If the report has been assigned any other report numbers *(either by the originator or by the sponsor)*, also enter this number(s).

10. AVAILABILITY/LIMITATION NOTICES: Enter any limitations on further dissemination of the report, other than those imposed by security classification, using standard statements such as:

(1) "Qualified requesters may obtain copies of this report from DDC."

(2) "Foreign announcement and dissemination of this report by DDC is not authorized."

(3) "U. S. Government agencies may obtain copies of this report directly from DDC. Other qualified DDC users shall request through _____."

(4) "U. S. military agencies may obtain copies of this report directly from DDC. Other qualified users shall request through _____."

(5) "All distribution of this report is controlled. Qualified DDC users shall request through _____."

If the report has been furnished to the Office of Technical Services, Department of Commerce, for sale to the public, indicate this fact and enter the price, if known.

11. SUPPLEMENTARY NOTES: Use for additional explanatory notes.

12. SPONSORING MILITARY ACTIVITY: Enter the name of the departmental project office or laboratory sponsoring *(paying for)* the research and development. Include address.

13. ABSTRACT: Enter an abstract giving a brief and factual summary of the document indicative of the report, even though it may also appear elsewhere in the body of the technical report. If additional space is required, a continuation sheet shall be attached.

It is highly desirable that the abstract of classified reports be unclassified. Each paragraph of the abstract shall end with an indication of the military security classification of the information in the paragraph, represented as *(TS), (S), (C), or (U)*.

There is no limitation on the length of the abstract. However, the suggested length is from 150 to 225 words.

14. KEY WORDS: Key words are technically meaningful terms or short phrases that characterize a report and may be used as index entries for cataloging the report. Key words must be selected so that no security classification is required. Identifiers, such as equipment model designation, trade name, military project code name, geographic location, may be used as key words but will be followed by an indication of technical context. The assignment of links, roles, and weights is optional.

SHIP RESEARCH COMMITTEE
Maritime Transportation Research Board
National Academy of Sciences-National Research Council

The Ship Research Committee has technical cognizance of the inter agency Ship Structure Committee's research program:

PROF. R. A. YAGLE, Chairman, *Prof. of Naval Architecture, University of Michigan*

DR. H. N. ABRAMSON, *Director Department of Mechanical Sciences, Southwest Research Inst.*

MR. W. H. BUCKLEY, *Chief Structural Criteria and Loads, Bell Aerosystems Co.*

DR. D. P. CLAUSING, *Senior Scientist, U.S. Steel Corporation*

MR. A. E. COX, *Senior Program Manager, Newport News Shipbuilding & Dry Dock Co.*

MR. J. F. DALZELL, *Senior Research Engineer, Stevens Institute of Technology*

DR. W. D. DOTY, *Senior Research Consultant, U. S. Steel Corporation*

MR. F. D. DUFFEY, *Welding Engineer, Ingalls Shipbuilding Corporation*

MR. D. FAULKNER, *Research Associate, Massachusetts Institute of Technology*

PROF. W. J. HALL, *Prof. of Civil Engineering, University of Illinois*

MR. J. E. HERZ, *Chief Structural Design Engineer, Sun Shipbuilding & Dry Dock Co.*

MR. G. E. KAMPSCHAEFER, JR., *Manager, Application Engineering, ARMCO Steel Corporation*

PROF. B. R. NOTON, *Prof. of Aerospace & Civil Engineering, Washington University*

MR. W. W. OFFNER, *President, X-ray Engineering International, Atomic Supply Corporation*

CDR R. M. WHITE, USCG, *Chief, Applied Engineering Section, U.S. Coast Guard Academy*

MR. R. W. RUMKE, *Executive Secretary, Ship Research Committee*

Advisory Group II, "Ship Structural Design" prepared the project prospectus and evaluated the proposals for this project.

MR. J. E. HERZ, Chairman, *Chief Structural Design Engineer, Sun Shipbuilding & Dry Dock Co.*

MR. A. E. COX, *Senior Program Manager, Newport News Shipbuilding & Dry Dock Co.*

MR. D. FAULKNER, *Research Associate, Massachusetts Institute of Technology*

PROF. J. E. GOLDBERG, *Prof. of Civil Engineering, Purdue University*

PROF. B. R. NOTON, *Prof. of Aerospace & Civil Engineering, Washington University*

PROF. J. R. PAULLING, JR., *Prof. & Chairman of Department of Naval Architecture, University of California*

MR. D. P. ROSEMAN, *Naval Architect, Hydronautics, Inc.*

CDR R. M. WHITE, USCG, *Chief, Applied Engineering Section, U.S. Coast Guard Academy*

The SR-193 Project Advisory Committee provided the liaison technical guidance, and reviewed the project reports with the investigator

PROF. J. E. GOLDBERG, Chairman, *Professor of Civil Engineering, Purdue University*

PROF. S. T. ROLFE, *Civil Engineering Department, University of Kansas*

MR. JOHN VASTA, *Senior Consultant, Litton Systems, Inc. A.M.T.D.*

SHIP STRUCTURE COMMITTEE PUBLICATIONS

These documents are distributed by the Clearinghouse, Springfield, Va. 22151. These documents have been announced in the Clearinghouse journal U.S. Government Research & Development Reports (USGRDR) under the indicated AD numbers.

SSC-202, *Midship Wave Bending Moment in a Model of the Cargo Ship "California Bear" Running at Oblique Headings in Regular Waves* by E. Numate and W. F. Yonkers. November 1969. AD 698847.

SSC-203, *Annual Report of the Ship Structure Committee.* November 1969. AD 699240.

SSC-204, *Simulated Performance Testing for Ship Structure Components* by R. Sherman. 1970. AD 705398.

SSC-205, *Structural Design Review of Long, Cylindrical, Liquid-Filled Independent Cargo Tank Barges* by C. W. Bascom. 1970. AD 708565.

SSC-206, *Permissible Stresses and Their Limitations* by J. J. Nibbering. AD 710520.

SSC-207, *Effect of Flame and Mechanical Straightening on Material Properties of Weldments* by H. E. Pattee, R. M. Evans, and R. E. Monroe. 1970. AD 710521.

SSC-208, *Slamming of Ships: A Critical Review of the Current State of Knowledge* J. R. Henry and F. C. Bailey. 1970. AD 711267.

SSC-209, *Results From Full-Scale Measurements of Midship Bending Stresses on Three Dry Cargo Ships* by I. J. Walters and F. C. Bailey. 1970. AD 712183.

SSC-210, *Analysis of Slamming Data from the "S. S. Wolvering State"* by J. W. Wheaton, C. H. Kano, P. T. Diamant, F. C. Bailey. 1970.

SSC-211, *Design & Installation of a Ship Response Instrumentation System Aboard the Container Vessel "S. S. Boston,* by R. A. Fain, J. Q. Cragin, and B. H. Schofield. 1970.

SSC-212, *Ship Reponse Instrumentation Aboard the Container Vessel "S. S. Boston": Results from the 1st Operational Season in North Atlantic Service* by R. A. Fain, J. Q. Cragin, and B. H. Schofield. 1970. AD 712186.

SSC-213, *A Guide for Ultrasonic Testing and Evaluation of Weld Flaws* by R. A. Youshaw. 1970.

SSC-214, *Ship Response Instrumentation Aboard the Container Vessel "S.S. Boston": Results from 2 Operational Seasons in North Atlantic Service* by J. Q. Cragin. 1970. AD 712187.

SSC-215, *A Guide for the Synthesis of Ship Structures Part One- The Midship Hold of a Transversely-Framed Dry Cargo Ship* by Manley St. Denis. 1970.